NAVAL POSTGRADUATE SCHOOL

MONTEREY, CALIFORNIA

THESIS

THE USE OF COMMERCIAL REMOTE SENSING IN PREDICTING HELICOPTER BROWNOUT CONDITIONS

by

Anthony Davis

September 2007

Thesis Advisor:	Richard Olsen
Second Reader:	Dave Trask

Approved for public release; distribution is unlimited

THIS PAGE INTENTIONALLY LEFT BLANK

REPORT DOCUMENTATION PAGE			*Form Approved OMB No. 0704-0188*
Public reporting burden for this collection of information is estimated to average 1 hour per response, including the time for reviewing instruction, searching existing data sources, gathering and maintaining the data needed, and completing and reviewing the collection of information. Send comments regarding this burden estimate or any other aspect of this collection of information, including suggestions for reducing this burden, to Washington headquarters Services, Directorate for Information Operations and Reports, 1215 Jefferson Davis Highway, Suite 1204, Arlington, VA 22202-4302, and to the Office of Management and Budget, Paperwork Reduction Project (0704-0188) Washington DC 20503.			
1. AGENCY USE ONLY ***(Leave blank)***	**2. REPORT DATE** September 2007	**3. REPORT TYPE AND DATES COVERED** Master's Thesis	
4. TITLE AND SUBTITLE The Use of Commercial Remote Sensing Predicting Helicopter Brownout Conditions			**5. FUNDING NUMBERS**
6. AUTHOR(S) Anthony Davis			
7. PERFORMING ORGANIZATION NAME(S) AND ADDRESS(ES) Naval Postgraduate School Monterey, CA 93943-5000			**8. PERFORMING ORGANIZATION REPORT NUMBER**
9. SPONSORING /MONITORING AGENCY NAME(S) AND ADDRESS(ES) N/A			**10. SPONSORING/MONITORING AGENCY REPORT NUMBER**
11. SUPPLEMENTARY NOTES The views expressed in this thesis are those of the author and do not reflect the official policy or position of the Department of Defense or the U.S. Government.			
12a. DISTRIBUTION / AVAILABILITY STATEMENT Approved for public release; distribution is unlimited			**12b. DISTRIBUTION CODE**

13. ABSTRACT (maximum 200 words)

Observations of potential helicopter landing zones are analyzed to determine suitability with respect to helicopter brownout. Imagery from civil and commercial satellites is used. VNIR and LWIR imagery of Yuma Proving Grounds taken by the ASTER sensor are analyzed. NDVI calculations from the VNIR data are used to define bare earth and vegetated areas. Some correlation is found in LWIR signatures, but the 60-m GSD for those bands limits utility. QuickBird MSI taken over Iraq is also analyzed for vegetation; results could not be ground truthed.

14. SUBJECT TERMS ASTER, QuickBird, NDVI, VNIR, LWIR			**15. NUMBER OF PAGES** 93
			16. PRICE CODE
17. SECURITY CLASSIFICATION OF REPORT Unclassified	**18. SECURITY CLASSIFICATION OF THIS PAGE** Unclassified	**19. SECURITY CLASSIFICATION OF ABSTRACT** Unclassified	**20. LIMITATION OF ABSTRACT** UU

NSN 7540-01-280-5500

Standard Form 298 (Rev. 2-89)
Prescribed by ANSI Std. 239-18

THIS PAGE INTENTIONALLY LEFT BLANK

Approved for public release; distribution is unlimited

THE USE OF COMMERCIAL REMOTE SENSING IN PREDICTING HELICOPTER BROWNOUT CONDITIONS

Anthony W Davis Jr
Lieutenant, United States Navy
B.S. Morehouse College 2001

Submitted in partial fulfillment of the
Requirements for the degree of

MASTER OF SCIENCE IN SPACE SYSTEMS OPERATIONS

from the

NAVAL POSTGRADUATE SCHOOL
September 2007

Author: Anthony Davis

Approved by: Richard Olsen
Thesis Advisor

David Trask
Second Reader

Rudolf Panholzer
Chairman, Space Systems Academic Group

THIS PAGE INTENTIONALLY LEFT BLANK

ABSTRACT

Observations of potential helicopter landing zones are analyzed to determine suitability with respect to helicopter brownout. Imagery from civil and commercial satellites is used. VNIR and LWIR imagery of Yuma Proving Grounds taken by the ASTER sensor are analyzed. NDVI calculations from the VNIR data are used to define bare earth and vegetated areas. Some correlation is found in LWIR signatures, but the 60-m GSD for those bands limits utility. QuickBird MSI taken over Iraq is also analyzed for vegetation; results could not be ground truthed.

THIS PAGE INTENTIONALLY LEFT BLANK

TABLE OF CONTENTS

LIST OF FIGURES

THIS PAGE INTENTIONALLY LEFT BLANK

LIST OF TABLES

THIS PAGE INTENTIONALLY LEFT BLANK

ACKNOWLEDGMENTS

First and foremost the author would like to thank his family for their continued sacrifice while a student at Naval Postgraduate School. Secondly, the author would like to thank Dr. Richard C Olsen for his training and guidance throughout the thesis process. The author would also like to thank the BOA team for allowing him to contribute to the BOA project in particular Lt. Col. Mitch “Rico” Rios and Rick Galbraith. Last but not least the author would like to thank research assistant, Angela Puetz, for all her help with the software used in this thesis.

THIS PAGE INTENTIONALLY LEFT BLANK

I. INTRODUCTION

A. OVERVIEW

In aviation, a **brownout** (or *brown-out*) is an in-flight visibility limitation due to dust or sand in the air. In a brownout, the pilot cannot see close proximity objects which offer the outside visual positions necessary to control the aircraft near the ground. This can cause spatial disorientation and loss of situational awareness leading to an accident. Pilots have compared landing during brownouts to parallel parking an automobile with your eyes closed. (Brownout (aviation) 2007)

The brownout phenomenon causes accidents during helicopter landing and take-off operations in arid desert terrain. Intense, blinding dust clouds swirl up by the helicopter rotor downwash during near-ground flight causes significant flight safety risks from aircraft and ground obstacle collisions, and dynamic rollover due to sloped and rough terrain. Brownouts have claimed more helicopters in recent military operations than all other threats combined.

There are numerous aspects which influence the probability and severity of brownout:

- rotor disk loading
- rotor configuration
- soil composition
- wind
- approach speed and angle

“Blowing sand and dust can cause a false impression of a tilted horizon. A pilot not using the flight instruments as a reference may intuitively try to level the aircraft with respect to the false horizon, resulting in an accident.” (Brownout (aviation) 2007) Helicopter rotor wash also causes sand to blow around outside the cockpit windows, possibly leading the pilot to experience the vection illusion, where the helicopter appears

to be turning when it is actually in a level hover. This can also cause the pilot to make incorrect control inputs, which can quickly lead to disaster when hovering near the ground.

In night landings, aircraft lighting can enhance the visual illusions by illuminating the brownout cloud. “Another phenomenon observed at night is "Pixie dust" caused by small particles hitting the leading edge of the rotor blades and making tiny sparks, creating a disk-shaped sparkling glow around the rotor.” (Brownout (aviation) 2007) This effect can also produce spatial disorientation in the uninitiated pilot.

Several coalition military aircraft were lost due to roll-overs while executing dust landings during the Gulf War period of 1990-91. In the decade between then and Operation Enduring Freedom, the U.S. Army recorded over 40 cases of brownout condition accidents during training at the Fort Irwin Military Reservation National Training Center in California, and other various sites. (Brownout (aviation) 2007) Since 1991, there have been over 230 cases of aircraft damage and/or injury due to unsuccessful take-offs or landings in a dust environment. Although most incidents occur during landings, there have been a significant number of incidents occurring during take-offs as well. “For the more than 50 brown-out incidents with damage reported to date during Army military operations in the 2001-2007 time frame, 80 percent were during landings and 20 percent during takeoffs.” (Brownout (aviation) 2007)

Helicopter brownout is a US$100 Million per year problem for the U.S. Military in Afghanistan and Iraq. The Army reports over 3/4th of helicopter accidents can be linked to brownout. Brownout accidents occur at close proximity e to the ground and at low airspeed, giving these accidents a higher survivability than other types. However, there have been deaths in military accidents in Iraq and Afghanistan, and nearly all of those were preventable. (Brownout (aviation) 2007)

B. BROWNOUT PHENOMENON REVISITED

Brownout (whiteout when caused by snow) is the condition when the helicopter rotor system creates a downward flow of air that disturbs the soil below it, forcing the dust and sand into the air, which prevents the pilot or aircrew from maintaining sufficient

ground and obstacle reference to make a safe landing or to safely maneuver the helicopter while in close proximity to the ground. Brownout is related to the rotor downwash associated with a hovering helicopter. The air is blown directly down from the rotor disc to the ground. From here the air flows out from below the helicopter and as it clears the direct down wash it is able to climb up and away from the ground causing a cloud of dust and sand to form all around the helicopter.

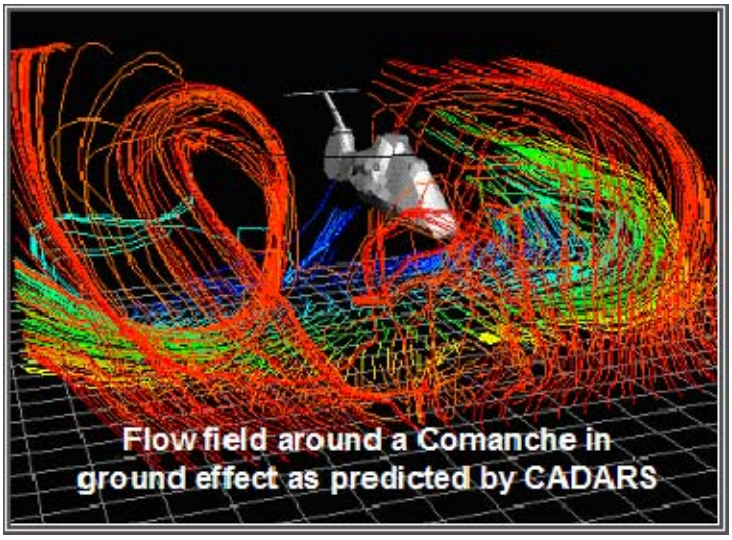

Figure 1. Ground effect prediction by CADARS (from *CDI - products.*)

Figure 2 shows dust and sand being disturbed by the rotor downwash. Some of this dust and sand then becomes re-circulated, drawn back through the rotor system and further impairing the pilot's visibility. Once ground references are lost the pilot can no longer identify and therefore correct for the drift of the helicopter which can result in impacting obstacles and other aircraft, or landing with too much momentum and damaging the landing gear or rolling the helicopter over on landing.

Figure 2. Soil caught in rotor downwash, start of brownout (from *Brownout California soil resource lab)*

. A second issue associated with brownout conditions is the affect the dust and sand has on the engines and rotors of the helicopter. The engines can experience numerous problems associated with the turbines and overall airflow. The rotors experience accelerated erosion and wear on blade edges and linkages. Unsurprisingly there is an increased need for maintenance when operating in brownout conditions on a recurring basis. (Shewfelt 2006)

A closing consideration for forecasting brownout conditions for avoidance is in the range of extraordinary/clandestine operations. The cloud produced by a helicopter with major downwash can send a cloud of dust and silt hundreds of feet into the air. The helicopter may have been heard but not seen, yet the brownout cloud can be seen for quite a distance.

C. BROWNOUT SURVEY

A Brownout survey was established by Major Shewfelt USMC. It was created to aid in the location, collection and analysis of brownout conditions. This was created to allow helicopter pilots and aircrew from all services to provide input as to their experiences and evaluation of landing zones that have been encountered through training and operations. The site was established through Naval Post graduate school utilizing the SurveyMonkey.com website services. The survey is presently developed for unclassified interface and is not partial to the number of times an individual can visit the site and update or supply new information. (Shewfelt 2006)

(U) An example of the survey is shown in the appendix and was design to be simple and requires minimal typing. It can be completed in less than nine minutes so not to discourage participation. It requests the following information:

(U) Point of Contact information- primarily to coordinate site visits

(U) General Operating Area and Profile

(U) Specific Landing Zone Locations

(U) Brownout Landing Zone

(U) Non-Brownout Landing Zone

(U)Landing Zone Descriptions

(U) Remarks

This information will help to build a data base of evaluated sites with the consideration that a solid algorithm will be established that can be applied to any potential landing zone. The following links are available to access the survey:

Take survey/ Provide input

http://www.surveymonkey.com/s.asp?u=888532045346

Access Survey Data

http://www.surveymonkey.com/Report.asp?U=204534935961

The NRL and NRO are currently working on establishing a secret level website for deployed units to provide feedback on operational sites. Through the use of the survey, numerous agencies may take advantage of the information to support various types of research that are being conducted in the effort to minimize or prevent brownout.(Shewfelt 2006)

D. GOALS

The Goal of this thesis is to do terrain classification for the purpose of predicting brownout conditions. Civil systems will be used to look at visible and infrared signatures of different terrain types. Chapter 2 looks at soil moisture theory, some basics on Remote Sensing, and the remote sensing instruments used in this thesis. Chapter 3 discusses the data acquisitions sites, remote sensing technology and evaluation techniques. Chapter 4 shows the observations and analysis of the data.

II. BACKGROUND

A. SOIL MOISTURE

This chapter is meant as a review of previous background in soil moisture. Prior thesis work by LTCOL Rios and MAJ Shewfelt go into the details of soil composition. This is a brief summary how moisture is collected and retained near and on soil. It is necessary to review this for it is the scientific foundation for why this thesis will work This section will also summarize vegetation and moisture sensing via the electromagnetic spectrum.

Name of soil separate	**Diameter limits (mm)**
Very coarse sand*	2.00 - 1.00
Coarse sand	1.00 - 0.50
Medium sand	0.50 - 0.25
Fine sand	0.25 - 0.10
Very fine sand	0.10 - 0.05
Silt	0.05 - 0.002
Clay	less than 0.002
* Note that the sand separate is split into five sizes (very coarse sand, coarse sand, etc.). The size range for sands, considered broadly, comprises the entire range from very coarse sand to very fine sand, i.e., 2.00-0.05 mm.	

Table 1. Size limits (diameter in millimeters) of soil separates in the USDA soil textural classification system.(After Shewfelt 2006)

1. Soil and Water Interaction

Soils have different textures and with that as shown in Figure 4 soils have different sizes also. Soils have pores that are filled with air and water. Soils with large pores have been found to allow water to drain through by gravity or percolate down through the soil. Soils with small pores will impede or prevent the water from percolating

through the soil.(Shefelt 2006) Water holding capacity of a soil is based on its surface area and pore space. Therefore finer soils like silt loam have a higher water holding capacity and sand which has a larger particle size does not. Colloids are very small particles within the soils that are between 5nm and 0.2 microns in diameters. Colloids can be hydrophobic which do not interact with water or hydrophilic which does interact well with water. Molecules of a **hydrophilic colloid** have an affinity for water molecules and when dispersed in water become hydrated. Hydrated colloids swell and increase the viscosity of the system, thereby improving stability by reducing the interaction between particles and their tendency to settle. (Shewfelt 2006) They may also possess a net surface electrical charge. The charge sign depends on the chemical properties of the colloid and the pH of the system. The presence of a surface charge produces repulsion of the charged particles and thus reduces the likelihood that the particles will adhere to one another and settle.

Adhesion and cohesion plays a role in the ability of the soil to retain moisture. Adhesion applies to the attraction of the water molecules to the surfaces of the soil and cohesion would refer to the attraction of the water molecules to one another. These two forces provide for the capillary effect which would resist the percolation of the water, and also provide for the process of binding or aggregating the soil as the water evaporates. Aggregating is the process by which as water molecules evaporate and the bond s become shorter, the soil particles are drawn closer together to the point that there are no longer any water molecules present but now the soil has bonded together. (Shewfelt 2006 as cited in Brady and Nyle 2004) The strength of that bond will be dependent upon the type of soil. Clays will form stronger bonds as can be seen in hard packed clay roads, while sand will exhibit nearly no bonding much like beach sand.

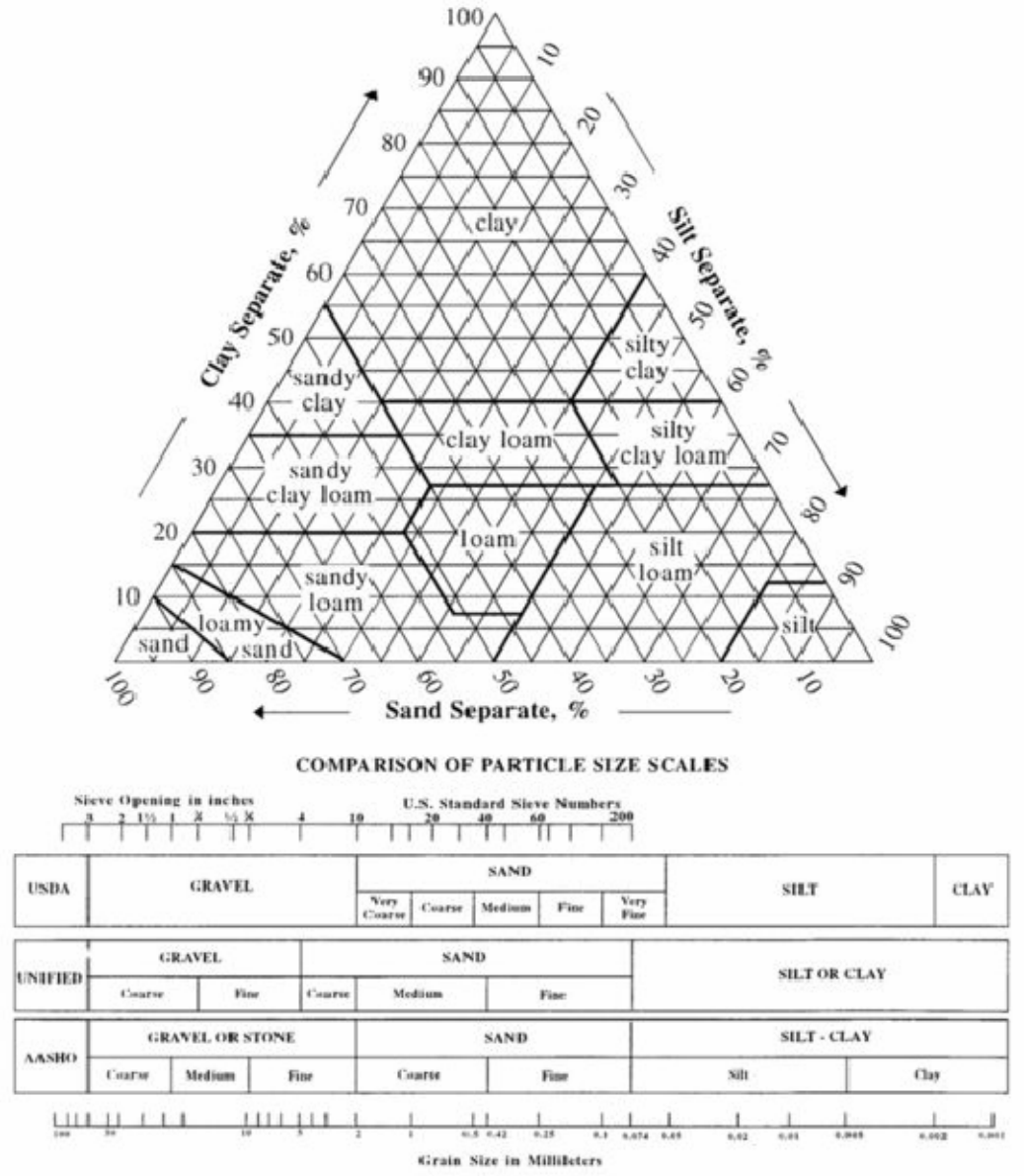

Figure 3. Sand particle pyramid (From Comparison of particle size scale)

2. Vegetation

Vegetation can indicate the presence of water, and serves the helicopter pilot by providing good visual reference points for landing. The discussion about soil moisture all leads to vegetation in a given region. Vegetation can be a good representation of the capacity of the soil to retain moisture. Sparse vegetation, which is common in arid and semi-arid regions, is generally due to the limited amount of precipitation and the fact that

most of the precipitation received does not penetrate very deep into the ground. That which does percolate into the ground is generally taken up by the plant roots during the summer months and eventually lost via transportation. For this case, there is not a great amount of retained water to support an abundant plant life. In humid temperate regions where soil is more amenable to water penetration and percolation, thicker larger collections of plant life is possible because enough water is held in the soil to support life during the dryer months.(Shewfelt 2006)

The above background information can be summarized by saying the health of the vegetation in a given area is directly dependent on the amount of water it received. The more water a plant receives the more chlorophyll it can generate. Chlorophyll is the compound in the leaves that makes the leaves green in color. Having sufficient amounts of water will provide for healthy green leaves as well as promote new growth of more green vegetation.(Shewfelt 2006) This green leaf vegetation relation to moisture plays a vital role in identifying a cursory assessment relative dryness or moistness of an area and is the scientific basis of this thesis.

B. MOISTURE SENSING VIA THE ELECTROMAGNETIC SPECTRUM

1. Electromagnetic Spectrum

The electromagnetic (EM) spectrum is very sensitive to water or moisture, in the atmosphere as well as the ground. Certain regions of the spectrum are completely attenuated by water in the air and are only useful from the upper atmosphere and higher or at very short range with high power.

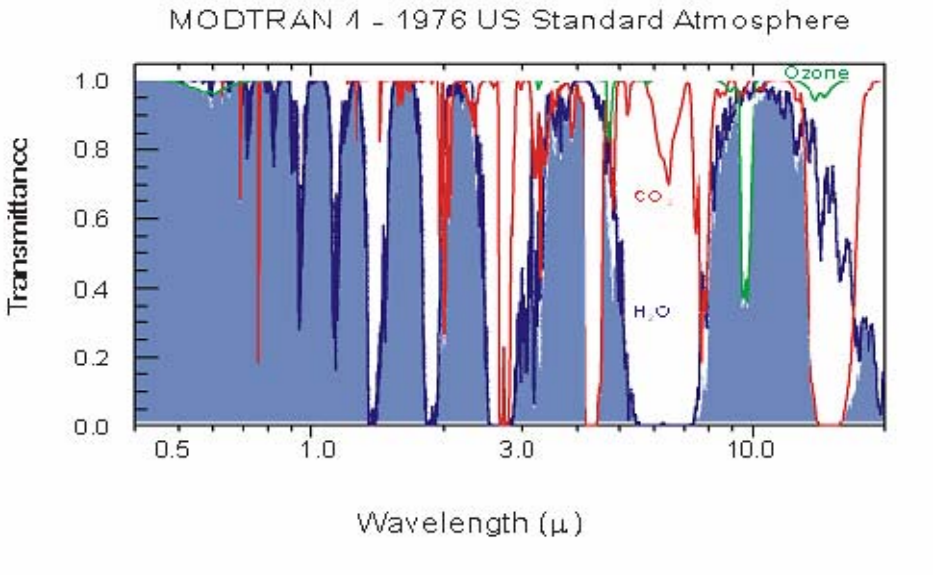

Figure 4. Atmosphere Absorption Regions of Spectral Bands (From Olsen 2007)

2. Applications and Limitations

The visible band of the EM spectrum (0.4 μm to 0.7μm) is sufficient to identify macro level changes in surface and soil moisture such as floods, droughts, and erosion. Practice would say the lighter colors imply dry and darker colors imply wet, this does not hold true when observing dissimilar adjacent materials that are naturally different in color. An example of this would be a volley ball court with white beach sand surrounded by darker agricultural soil.(Shewfelt 2006) Wet beach sand would still appear lighter than the surrounding agricultural soil of the same dampness. The use of color differences is limited in such instances as autumn when the leaves have covered the ground and color variation in the soil color is not observable.

The near infrared band of the EM spectrum (NIR) is from 0.75μm to 1.0μm. This band is where the chlorophyll characteristics of vegetation are detected. The chlorophyll is highly reflective in the NIR band, and as was discussed before the healthier plants with sufficient watering and soil moisture will produce more chlorophyll and show brighter in

a NIR image. Figure 5 below shows the USGA spectral library for vegetation shows the reflectance for different vegetation types. The green arrow shows what is called the IR ledge which is the reason why healthy vegetation appears red in “false color” NIR images.

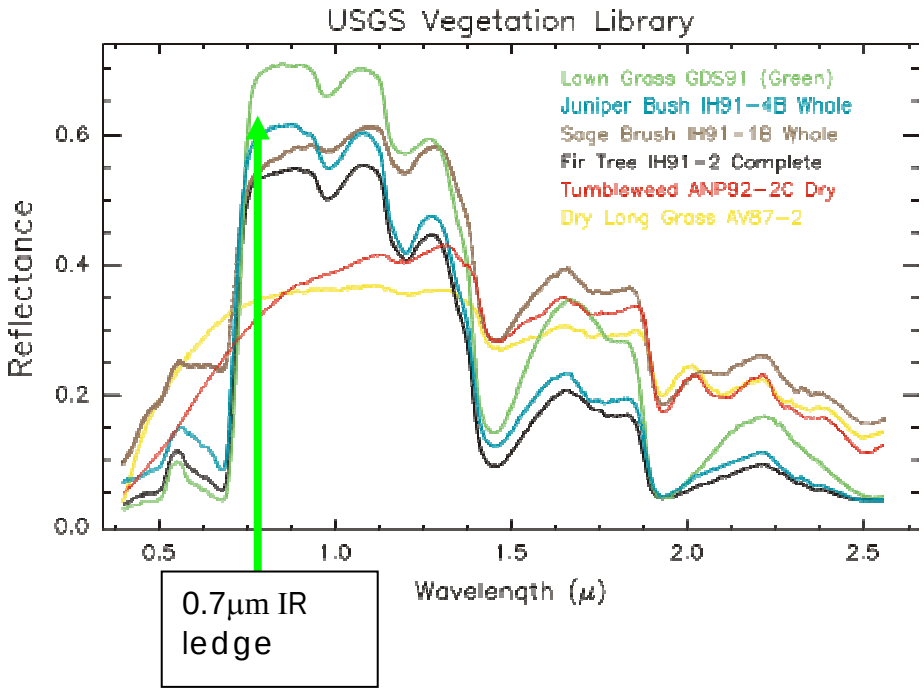

Figure 5. USGS Vegetation Library(From Olsen, 2007)

Thermal IR is generally acquired in two bands when used in remote sensing, Medium Wave IR (MWIR, 3 μm to 5μm) and Long Wave IR (LWIR, 8μm to 14μm).MWIR is sensitive to both reflected sunlight (during the day), and thermally emitted radiation .LWIR are largely independent of reflected sunlight, and offer more possibilities for they study the effects of thermal inertia. The emmissivity of an object is the amount of radiant energy it emits at a given wavelength. Table 1 shows the emmissivity of some common materials in the LWIR.(Olsen 2007) When IR is applied for moisture detection, the thermal inertia of the objects in an image is the focus. Thermal inertia is the ability of a substance to resist temperature change. This is a function of density and thermal capacity (ability of a substance to store heat) and thermal

conductivity (the rate at which a substance conducts heat). As can be seen in Table 2, the thermal inertia of water is higher than that of sand or dry wood. So if moisture was present in wet sand (wet soil) the thermal inertia of these substances would be higher and hence overall temperature change would be smaller in a temperature cycle. If an area of just sand and rock was imaged, the measure of moisture in the sand (more capable of retaining moisture) would be compared to the rock, which is less likely to retain moisture, and further compared to a day when the same sand was dry. Moist soil would have a smaller temperature variation from the rocks than would dry soil over the same twenty-four hour period. The changes are not large but when viewed in IR the differences can be easily evaluated.

Material	Emissivity
Granite	0.815
Sand, quartz, large-grain	0.914
Asphalt, paving	0.959
Concrete walkway	0.966
water, with thin layer of petroleum	0.972
Water, pure	0.993

Table 2. Emissivities of common materials(From Olsen 2007)

Material	$K\left(\frac{\text{calories}}{\text{cm s }^{\circ}\text{C}}\right)$	$C\left(\frac{\text{calories}}{\text{gm }^{\circ}\text{C}}\right)$	$\rho\ \frac{gm}{cm^3}$	$P\left(\frac{\text{calories}}{\text{cm}^2\ ^{\circ}\text{C}\ s^{\frac{1}{2}}}\right)$
Water	0.0014	1.0	1.0	0.038
Wood (oak)	0.0005	0.33	0.82	0.012
Sand Soil	0.0014	0.24	1.82	0.024
Basalt	0.0045	0.21	2.80	0.053
Aluminum	0.538	0.215	2.69	0.544
Copper	0.941	0.092	8.93	0.879
Stainless Steel	0.030	0.12	7.83	0.168

Table 3. Thermal parameters of various materials (From Olsen 2007)

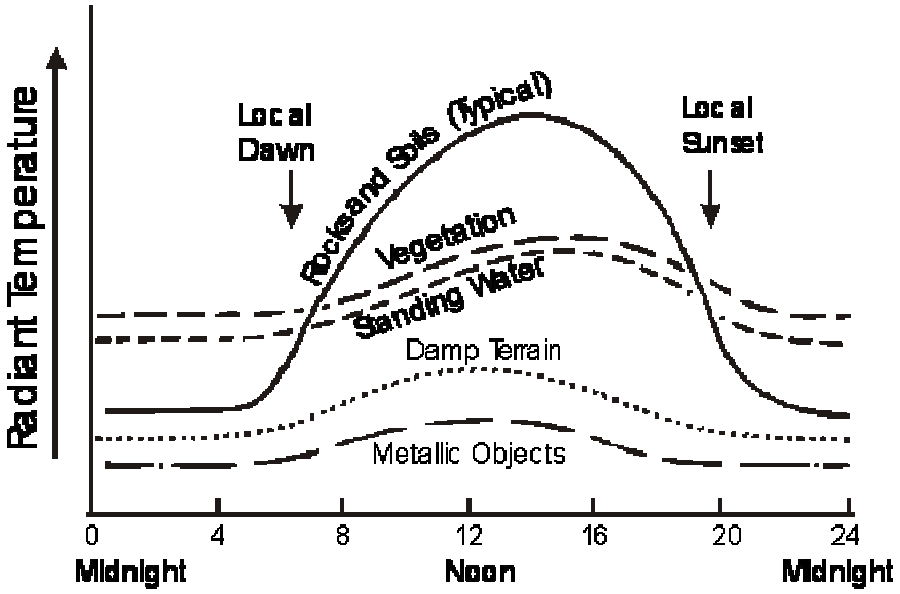

Figure 6. Illustration of the temporal variations in temperature for various materials over a day(From Olsen 2007)

"The thermal inertia of the vegetation, gravel (desert pavement), mountain rock, and paved runway associated with non brownout areas proved to be measurably higher than that of the brownout areas."(Olsen 2007) Loose dry soils have a low thermal inertial or resistance to temperature change, which means its temperature, will vary faster than other objects with higher thermal inertias. The table below lists thermal inertias that closely relate to the materials analyzed at YPG as well as other sites.

Material	Thermal Inertia [cal/(cm^2*°C*s½)]
Sand soil	0.024
Granite	0.056
Sandy Gravel	0.050
Gravel	0.033
Shale	0.041
Water (vegetation)	0.036

Table 4. Thermal inertias of Materials Similar to Site Material (From Shewfelt 2006)

Figure 6 shows the thermal inertia of common material in a twenty four hour period. There is a small temperature variance for damp soil, in contrast there is a substantial difference between the vegetation rocks and soils. This knowledge plays heavily into the science behind how this thesis works.

C. REMOTE SENSING INSTRUMENTS

1. ASTER

The Advanced Spaceborne Thermal Emission and Reflection Radiometer (ASTER) is an instrument built by Japanese (Ministry of International Trade and Industry MITI) and American (NASA/JPL) team. ASTER was launched on NASA's Earth Observing System morning (EOS-AM1) platform in 1998 the platform was subsequently renamed the TERRA satellite. “ASTER has three spectral bands in the visible near-infrared (VNIR), six bands in the shortwave infrared (SWIR), and five bands in the thermal infrared (TIR) regions, with 15-, 30-, and 90-m ground resolution, respectively.” (Yamaguchi, Kahle, Tsu, Kawakami, & Pniel, 1998) The VNIR subsystem has a rearward -viewing band for stereoscopic surveillance in the along-track direction. Because the data has wide spectral coverage and fairly high spatial resolution, it is possible to discriminate a variety of surface materials and reduce problems in some lower resolution data resulting from mixed pixels. ASTER provides high-spatial resolution multispectral thermal infrared data from orbit and the highest spatial resolution surface spectral reflectance temperature and emissivity data of all of the EOS-AM1 instruments. (Yamaguchi et al., 1998)

“The primary science objective of the ASTER mission is to improve understanding of the local- and regional-scale processes occurring on or near the Earth's surface and lower atmosphere, including surface-atmosphere interactions. Specific areas of the science investigation include the following: (1) land surface climatology; (2) vegetation and ecosystem dynamics; (3) volcano monitoring; (4) hazard monitoring; (5) aerosols and clouds; (6) carbon cycling in the marine ecosystem; (7) hydrology; (8) geology and soil; and (9) land surface and land cover change.” (Yamaguchi et al., 1998)

There are three categories of ASTER data: a global map, regional monitoring data sets, and local data sets to be obtained for requests from individual investigators. For this thesis we will look at two instruments payload on ASTER the VNIR and the TIR.

The VNIR subsystem functions in three spectral bands at visible and near-IR wavelengths, with a resolution of 15 m. The three VNIR bands have bandpasses similar to those of the Landsat Thematic Mapper (TM) and the Optical Sensor (OPS) of the Japanese Earth Resources Satellite (JERS-1). The VNIR is particularly useful for topographic understanding because it has along track stereo coverage in band 3, with nadir (band 3N) and backward band (3B). The VNIR bands are effective in measuring vegetation and iron-oxide minerals in soils and rocks.(Visible Near Infrared (VNIR) 2004)

"System design consists of two telescopes--one nadir-looking with a three-spectral-band detector, and the other backward-looking with a single-band detector. The backward-looking telescope offers the second view of the target area in Band 3 for stereo observations. Thermal control of the CCD detectors is provided by a platform-provided cold plate."(Visible Near Infrared (VNIR) 2004) Cross-track pointing to 24 degrees on both sides of the track is accomplished by spinning the entire telescope assembly. The data rate is 62 Mbps when all four bands are operating. Two on-board halogen lamps are used for calibration of the nadir-looking detectors. This calibration source is always in the optical path. (Visible Near Infrared (VNIR) 2004)

a. VNIR

The VNIR subsystem is comprised of two autonomous telescope assemblies to decrease image distortion in the backward and nadir looking telescopes. The detectors for each of the bands consist of 5000 element silicon charge coupled detectors (CCD's). Only 4000 of these detectors are used at any one time. A time lag occurs between the acquisition of the backward image and the nadir image. During this time earth rotation displaces the image center. The VNIR subsystem automatically extracts the correct 4000 pixels based on orbit position information supplied by the EOS platform."(Visible Near Infrared (VNIR) 2004)

The VNIR optical system is a reflecting-refracting improved Schmidt design. The backward looking telescope focal plane contains only a single detector array (Band 3 of Table II) and uses an interference filter for wavelength discrimination. The focal plane of the nadir telescope contains 3 line arrays and uses a dichroic prism and delay filters for spectral separation allowing all three bands to view the same area simultaneously. “The telescope and detectors are kept at 296 + 3K using thermal control and cooling from a platform provided cold plate.”(Visible Near Infrared (VNIR) 2004)

“The system signal-to-noise is controlled by specifying the NE ΔP to be < 0.5% referenced to a diffuse target with a 70% albedo at the equator during equinox. The absolute radiometric accuracy is to be + 4% or better.”(Visible Near Infrared (VNIR) 2004)

The VNIR subsystem produces by far the highest data rate of the three ASTER imaging subsystems. With all four bands operating (3 nadir and 1 backward) the data rate including image data, supplemental information and subsystem engineering data is 62 Mbps (Visible Near Infrared (VNIR) 2004).

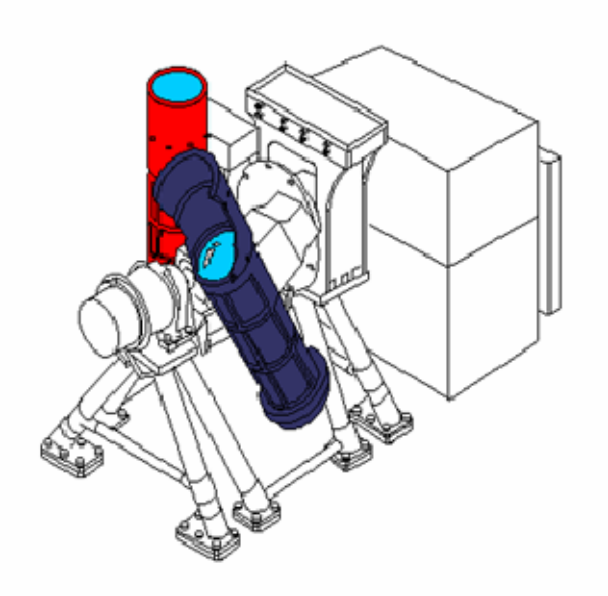

Figure 7. VNIR subsystem (From Visible Near Infrared (VNIR) 2004)

b. TIR

The TIR subsystem functions in five bands in the thermal infrared rang using a single, fixed-position, nadir-looking telescope with a resolution of 90 m. Emissivity models obtained from the five TIR bands are used to estimate silica content, which is significant in characterizing silicate rocks –the most abundant rock type on the earth's surface. "Distinct from the other instrument subsystems, it has a "whiskbroom" scanning mirror. Each band uses 10 detectors in a staggered array with optical bandpass filters over each detector element. The maximum data rate is 4.2 Mbps. The scanning mirror functions both for scanning and cross-track pointing (to ± 8.55 degrees)." (Thermal Infrared (TIR) 2004) In the scanning mode, the mirror oscillates at about 7 Hz and, during oscillation, data are collected in one direction only. During calibration, the scanning mirror rotates 90 degrees from the nadir position to view an internal black body. Because of the instrument's high data rate, restrictions have been imposed so that the average data rate is manageable by the spacecraft data management system. This restriction is a one-orbit maximum average rate of 16.6 Mbps and a two-orbit maximum average rate of 8.3 Mbps, which results in approximately a 9.3% duty cycle. (Thermal Infrared (TIR) 2004)

The TIR subsystem uses a Newtonian catadioptric system with an aspheric primary mirror and lenses for divergence improvement. Unlike the VNIR and SWIR telescopes, the telescope of the TIR subsystem is fixed with pointing and scanning done by a mirror. "Each band uses 10 Mercury-Cadmium-Telluride (HgCdTe) detectors in a staggered array with optical band-pass filters with each detector element. Each detector has its own pre-and post-amplifier for a total of 50. Performance of the system will be improved if photovoltaic detectors can be used. Development of such detectors is a technical challenge." (Thermal Infrared (TIR) 2004)

As with the SWIR subsystem, the TIR subsystem uses a mechanical split Stirling cycle cooler for maintaining the detectors at 80K. In this case, since the cooler is fixed, the waste heat it generates is removed using a platform supplied cold plate.

Thermal Infrared (TIR) (2004) states that the scanning mirror operates both for scanning and pointing. In the scanning mode the mirror oscillates at about 7 Hz. For calibration, the scanning mirror rotates 180 degrees from the nadir position to view an internal black body which can be heated or cooled. The scanning/pointing mirror design precludes a view of cold space, so at any one time only a one point temperature calibration can be effected. The system does contain a temperature controlled and monitored chopper to remove low frequency drift. In flight, a single point calibration can be done frequently (e.g., every observation) if necessary. On a less frequent interval, the black body may be cooled or heated (to a maximum temperature of 340K) to provide a multipoint thermal calibration. For the TIR subsystem, the signal-to-noise can be expressed in terms of an NE delta T. The requirement is that the NE ΔT be less than 0.3K for all bands with a design goal of less than 0.2K. The signal reference for NE ΔT is a blackbody emitter at 300K. The accuracy requirements on the TIR subsystem are given for each of several brightness temperatures ranges as follows: 200 - 240K, 3K; 240 - 270K, 2K; 270 - 340K, 1K; and 340 - 370K, 2K. The total data rate for the TIR subsystem, including supplementary telemetry and engineering telemetry, is 4.2 Mbps. Because the TIR subsystem can return useful data both day and night, the duty cycle for this subsystem has been set at 16%. The cryocooler, like that of the SWIR subsystem, operates with a 100% duty cycle. (para 1thur 5)

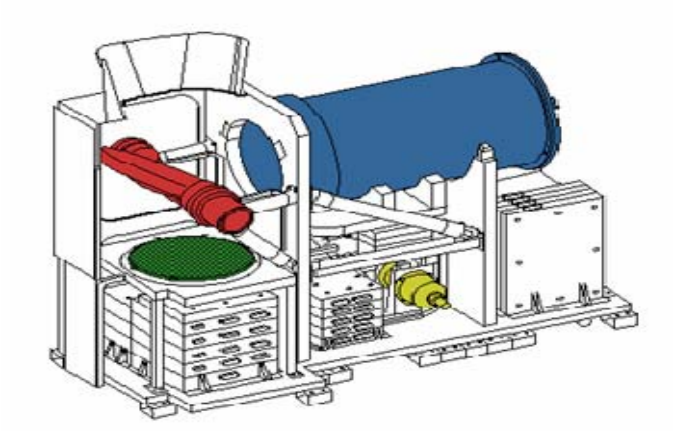

Figure 8. Diagram of TIR Payload (From Thermal Infrared (TIR) 2004)

c. Pointing Capabilities

All ASTER bands covers the same 60-km imaging swath with a pointing capability in the cross track direction to cover +/- 116 km from nadir, so that any point on the globe is accessible at least once every 16 days with the full spectral coverage provided by the VNIR, SWIR, and TIR. Three pointing positions (nadir, left, and right) are necessary to cover the earth's surface at the equator, where the EOS- AM1 orbit separation is 172 km. The use of the additional four intermediate pointing positions, which are located right on the boundaries of the swaths of the three nominal pointings, allows us to obtain smaller targets within a single scene, if the target is smaller than 60 km in diameter and located on the boundary of two of the three nominal swaths.

d. Operational Constraints

There are several constraints on ASTER data acquisition. Limitations on data acquisition derive from a variety of sources, including limits on the number of telescope pointing changes during mission, dissipation of heat, volume of data that can be stored in the EOS-AM1 solid state recorded, available power for ASTER, bandwidth of downlink, length of each downlink window, frequency of downlink window, and finally, the ability to schedule ASTER instrument activities.

The primary limitations on ASTER data collection are the data volume allocated to the instrument in the EOS-AM1's memory (solid-state recorder) and in the communications link with the Tracking and Data Relay Satellite System (TDRSS) and ground stations. The maximum average data rate allocated to ASTER, based on a two-orbit average is 8.3 Mbps, which roughly corresponds to 8 min of full mode daytime operation plus 8 min of nighttime TIR operation per orbit. "The single orbit maximum data acquisition time is 16 min, if no data is acquired in both pervious and following orbits. The peak data rate and peak power consumptions are 89.2 Mbps and 726 W, respectively. Given that the instrument is scheduled to operate for six years, ASTER could collect approximately 1.7 million scenes of full –mode data. In practice, there will be factors that will decrease this amount, such as scheduling inefficiencies. (Yamaguchi et al., 1998)

e Operation Modes

The three ASTER subsystems can be operated independently. In addition, there are several possible instrument gain settings and pointing angles. This results in many possible instrument gain settings and pointing angles. This results in many possible observation modes. However several nominal modes have been defined. The nominal daytime mode is simultaneous data acquisition using the three subsystems looking at the same 60-km imaging swath. The nominal nighttime mode is TIR-only operation. (Yamaguchi et al., 1998)

The daytime VNIR mode is used for areas where high-resolution VNIR data are essential, but SWIR (not used in thesis) and TIR spectral data are not necessary. In daytime stereo mode, only the bands 3N (nadir) and 3B (backward) operates for the purpose of stereo imaging. If a pointing angle of greater than 8.55 degrees is required, the daytime VNIR or stereo mode can be used, pointing out to +/- 24 degrees. The TIR mode is also accessible in the daytime. (Yamaguchi et al., 1998)

The open ocean is usually observed in the TIR mode since most ocean surface targets do not have interesting signatures in ASTER's VNIR or SWIR bands. These three modes (daytime VNIR, daytime stereo and daytime TIR) are complementary to the daytime full mode and will be used only when allocated resources cannot permit the full mode. An example of this, is periodic monitoring of the Antarctic glacier boundaries is one objective of the ASTER Science team was able to conduct and accomplished using the daytime stereo mode. (Yamaguchi et al., 1998)

Characteristic	VNIR	SWIR	TIR
Spectral Range	Band 1: 0.52 - 0.60 µm Nadir looking	Band 4: 1.600 - 1.700 µm	Band 10: 8.125 - 8.475 µm
	Band 2: 0.63 - 0.69 µm Nadir looking	Band 5: 2.145 - 2.185 µm	Band 11: 8.475 - 8.825 µm
	Band 3: 0.76 - 0.86 µm Nadir looking	Band 6: 2.185 - 2.225 µm	Band 12: 8.925 - 9.275 µm
	Band 3: 0.76 - 0.86 µm Backward looking	Band 7: 2.235 - 2.285 µm	Band 13: 10.25 - 10.95 µm
		Band 8: 2.295 - 2.365 µm	Band 14: 10.95 - 11.65 µm
		Band 9: 2.360 - 2.430 µm	
Ground Resolution	15 m	30m	90m
Data Rate (Mbits/sec)	62	23	4.2
Cross-track Pointing (deg.)	±24	±8.55	±8.55
Cross-track Pointing (km)	±318	±116	±116
Swath Width (km)	60	60	60
Detector Type	Si	PtSi-Si	HgCdTe
Quantization (bits)	8	8	12
System Response Function	VNIR Chart	SWIR Chart	TIR Chart
	VNIR Data	SWIR Data	TIR Data

ASTER bands superimposed on model atmosphere

Table 5. ASTER Characteristics (From Characteristics)

f ASTER Applications

Figure 9 shows a image chip of downtown London England and its associated Normalized Difference Vegetation Index (NDVI) transform. NDVI is a numerical ratio of the red and Near Infrared bands used in the measurement of vegetation in a given image and will be explained in greater detail later. The NDVI transform of

London shows that the bright green in the image indicates healthy vegetation in the London area and the darker green indicates sparse vegetation.

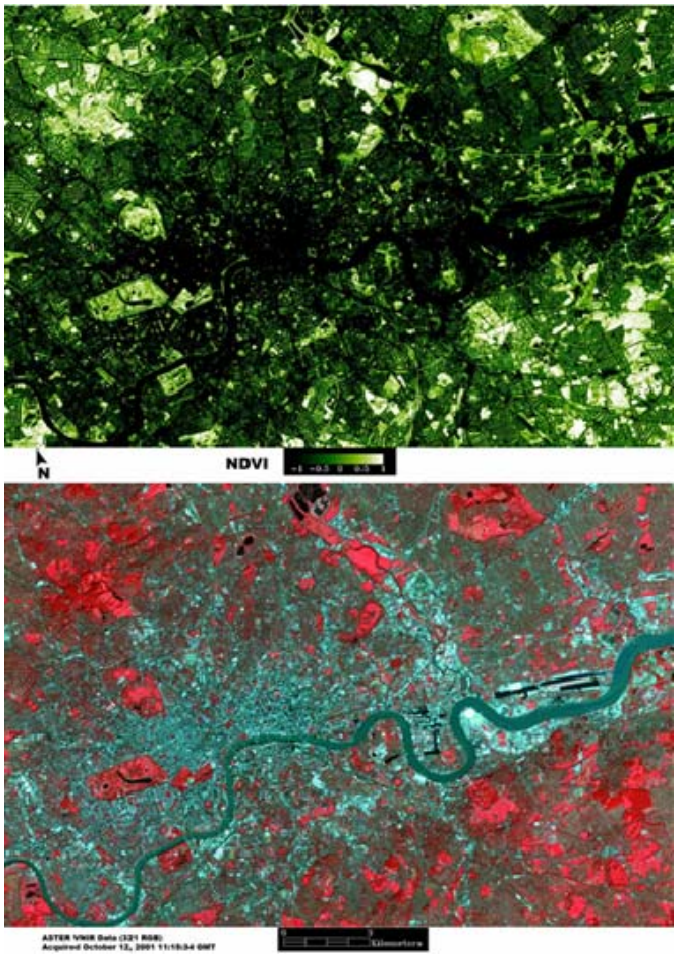

Figure 9. NDVI and ASTER VNIR data for downtown London metro area.(From Urban Change 2004)

Collection of multispectral thermal infrared data is a particular strength of ASTER. Nighttime data acquisitions over urban regions can be used to create maps of urban/peri-urban surface temperature that are invaluable for assessment of urban heat islands. The distribution of built materials throughout the urban landscape are of obvious importance in constructing thermal budgets, but consideration of the potential contributions of surrounding natural materials to the regional thermal budget is also important. For example, the Phoenix, AZ metropolitan area is surrounded by mountain

ranges with sparse vegetation cover; these ranges act as large thermal emitters during the night and have surface temperatures equivalent to urban core asphalt and concrete (Figure 10). This surface temperature information is valuable for investigation of urban climatic patterns and initialization of climate models. (Urban Changes 2004)

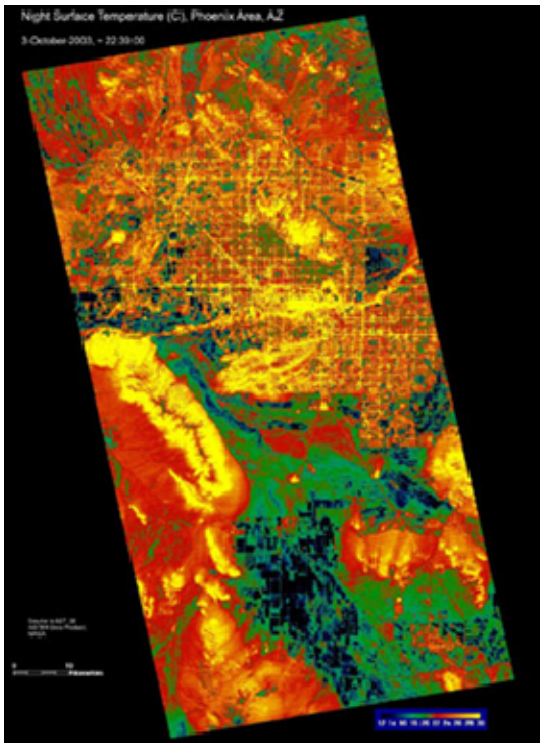

Figure 10. Surface temperature map of the Phoenix metropolitan area. North is to top of image. (From Urban Change 2004)

2. QuickBird

QuickBird is a high-resolution commercial earth observation satellite, owned by DigitalGlobe and launched in 2001 as the first satellite in a constellation of three scheduled to be in orbit by 2008. QuickBird collects the highest resolution commercial imagery of Earth, and boasts the largest image size and the greatest on-board storage capacity of any satellite. The satellite collects panchromatic (black & white) imagery at 60-70 centimeter resolution and multispectral imagery at 2.4- and 2.8-meter resolutions.

At this resolution, detail such as buildings and other infrastructure are easily visible. However, this resolution is insufficient for working with smaller objects such as a license plate on a car.

a. Design and Specifications

Orbit	Altitude: 450 km - 98 degree, sun-synchronous inclination Revisit frequency: 3-7 days depending on latitude at 60-centimeter resolution Viewing angle: Agile spacecraft - in-track and cross-track pointing Period: 93.4 minutes	
Per Orbit Collection	~128 gigabits (approximately 57 single area images)	
Swath Width & Area Size	Nominal swath width: 16.5-kilometers at nadir Accessible ground swath: 544-km centered on the satellite ground track (to ~30° off nadir) Areas of interest: Single Area - 16.5 km x 16.5 km Strip - 16.5 km x 165 km	
Metric Accuracy	23-meter circular error, 17-meter linear error (without ground control)	
Sensor Resolution & Spectral Bandwidth	Panchromatic 60-centimeter GSD (Ground Sample Distance) at nadir Black & White: 445 to 900 nanometers	Multispectral 2.4-meter GSD at nadir Blue: 450 to 520 nanometers Green: 520 to 600 nanometers Red: 630 to 690 nanometers Near-IR: 760 to 900 nanometers
Dynamic Range	11-bits per pixel	

Table 6. Design and Specifications chart DigitalGlobe QuickBird Specification(http://www.digitalglobe.com/about/quickbird.html)

THIS PAGE INTENTIONALLY LEFT BLANK

III. DATA ACQUISITION

Data was acquired from two different sites. One is a highly studied location of Yuma Proving Ground in Yuma Arizona. Yuma Proving Grounds is about 60 miles from Yuma. The other is random areas of Iraq taken by QuickBird.

These sites were selected upon the recommendations of helicopter pilots that had flown these sites and experienced brownout conditions in the course of there flight training. The YPG site being located in the southwestern part of the United States also tend to receive very little rain fall in the summer with temperature peaks at around 100 degrees Fahrenheit. This environment contributed well to the dry dusty settings for brownout to exist.

A. SITES

1. Locations

The table lists the landing zones sites evaluated for this thesis. At each site, multiple areas were identified for evaluation based on proximity, tendency toward brownout conditions, vegetation, and resistance to brownout conditions. Table 7 lists these sites and gives descriptions of the areas selected and the likely brownout capability. At each of the sites at least one area or landing zone was selected to allow for better comparison and contrast possibilities.

	7 Jul 06		Yuma Proving Ground, Arizona Brownout Test LZ
ypg_101	N33° 23.764' / W114° 16.575'.	Y-Worst Possible	Standing at center of 1000 sq meter test area. Soil has formed very thin crust easily broken with at least 3 inches of loose soil below.
ypg_102	N33° 23.764' / W114° 16.575'.	Y-Worst Possible	Same as above
ypg_103	N33° 23.764' / W114° 16.575'.	Y-Worst Possible	Same as above
ypg_104	N33° 23.764' / W114° 16.575'.	Y-Worst Possible	Same as above
ypg_105	N33° 24.025' / W114° 16.754'	N	Gravel LZ area to the N of the test area LZ. Ruler reference. Vehicle traffic did not disturb soil crust here.
ypg_106	N33° 24.025' / W114° 16.754'	N	Same as above
ypg_107	N33° 24.025' / W114° 16.754'	N	Same as above
ypg_108	N33° 24.025' / W114° 16.754'	N	Gravel LZ area to the N of the test area LZ. Looking north.
ypg_109	N33° 24.025' / W114° 16.754'	N	Gravel LZ area to the N of the test area LZ. Looking south toward brownout LZ area.
ypg_110	N33° 24.025' / W114° 16.754'	N	Gravel LZ area to the N of the test area LZ. Looking west across gravel LZ area.
ypg_111	N33° 23.859'/ W114° 16.458'	Y-Worst Possible	Standing at center of road intersection looking at SE quadrant. Former brownout test LZ tilled area.
ypg_112	N33° 23.859'/ W114° 16.458'	Y-light/ moderate	Standing at center of road intersection looking at NE quadrant. Some gravel but mostly underbrush and bushes. Estimate light to moderate brownout area. Crust similar to gravel LZ area.
ypg_113	N33° 23.859'/ W114° 16.458'	N	Standing at center of road intersection looking at NW quadrant. Gravel LZ area.
ypg_114	N33° 23.859'/ W114° 16.458'	Y-Worst Possible	Standing at center of road intersection looking at SW quadrant. Former brownout test LZ tilled area.

Table 7. Yuma Proving Grounds descriptions (From Shewfelt 2006)

Iraq was chosen for the second set of locations to be analyzed in this thesis. These locations include areas in Abu Dhakar, Al Qaim, Ar Rutbah, Al Asad, Anah, and Rawah for testing purposes. All Iraq images were taken by QuickBird.

2. Ground Truth

Ground truth measurements were taken at each sight of soil depth, crust thickness, and landing zones dimensions. Also recorded via photographs were general conditions of the sites, landing zones, vegetation, surrounding terrain and soil disturbed by a moving vehicle or helicopter when possible. Commercial hand held GPS devices were used to

mark the positions of the various landing zones. The other tools that were used by Shewfelt were a digital camera, ruler tape measure and U.S. Dollar bill and quarter (six inches x two inches and 3/4 inch respectively) for visual size reference.

Ground truth for Iraq does not exist for this iteration of the thesis but should be included for future studies in this subject.

3. Landing Zone Comparisons

a. Yuma Proving Grounds, Yuma, Arizona

The area observed at this site was initially set up in coordination with brownout testing being conducted by the Air Force Research Laboratory in support of the "Sand Blaster" research program.

There are two distinct areas assessed in support of this thesis. The first area or landing zone, YPG-LZ1, was identified as an extremely bad brownout landing zone. It is located at Lat/Long N33 23' 45.8"/W 114 16' 34.5". This landing zone area had been deliberately prepared by tilling the area repeatedly as part of the Sand Blaster research. After tilling, helicopters were scheduled to do low altitude passes at very slow airspeeds so that the tilled soil particles would be sent airborne and then collected by filters for further analysis. Figure 11 is a DigitalGlobe image of the area and it shows the tilled field clearly.

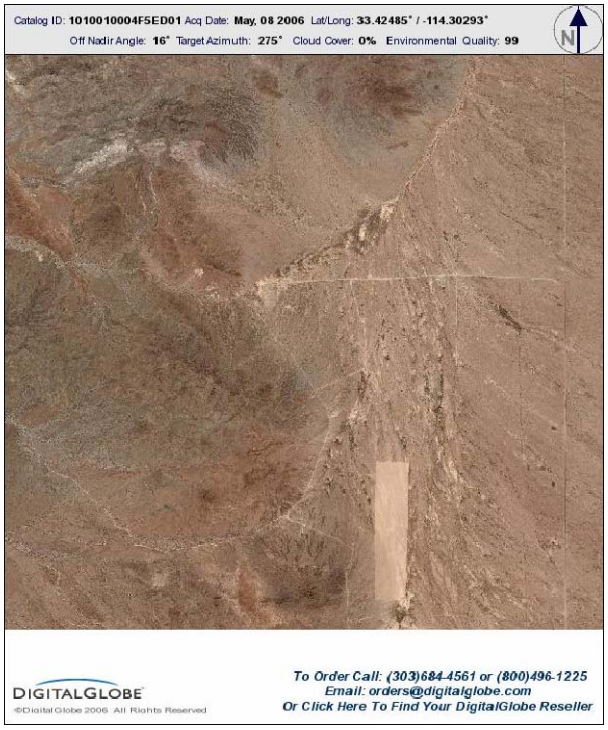

Figure 11. Digitalglobe image of Yuma Proving Ground

B. REMOTE SENSING TECHNOLOGY

ASTER level 1B images were purchased from NASA for the purposes of this thesis of Yuma Proving Ground also QuickBird data were obtained by NGA for 6 Iraqi sites that include Al-Asad, Abu-Dhakar, Al-Qaim, Ar-Rutbah, Anah, and Rawah.

C EVALUATION TECHNIQUES

1 Normalized Difference Vegetation Index (NDVI)

The NDVI is a calculation used to identify vegetation and its health through the levels of chlorophyll detected in the leaves. To achieve this the average reflectance values of NIR(0.75μm to 1.0μm) and red (0.6μm to 0.7μm) bands in a MSI image are applied to the following equation:

$$NDVI=(NIR-Red)/(NIR+Red)$$

The equation then provides a ratio of the change in reflectance of an object from the visible to the NIR in a scene, which allows evaluation of the level of chlorophyll present in plants and algae imaged. The ratios will range from -1.0 to+1.0. Higher ratios(>+0.5)represent significant healthy vegetation negative ratios (NDVI <0.0) represent little to no chlorophyll present i.e. barren soil. The plants which should be identifiable in the visible bands combined with this evaluation will be able to provide a rough estimate of the moisture present as well as the potential strength of the plants roots to hold the soil in place during helicopter operations.

2. 2D Scatter Plots

One can classify an image if the surface materials are known in certain regions these are referred to as training areas for classification. ENVI provides a 2D scatter plot tool that one can use to determine appropriate classification training areas.

ENVI's 2D scatter plot tool allows you to compare not only the relationship between data values in two bands but also the special distribution of pixels in an image. This combined functionality provides a very simple two band interactive classification of image data. For the purposes of this thesis the two band s we will look at is the NDVI and one of the five different spectral bands for the TIR subsystem.

THIS PAGE INTENTIONALLY LEFT BLANK

IV. ANALYSIS AND CONCLUSIONS

A MULTI-SPECTRAL IMAGERY

1. Yuma Proving Ground Analysis

a. ASTER Image Data

Archival ASTER data were selected from passes over Yuma Proving Ground (YPG). These passes included both day and nighttime images Table 8 shows the locations, and times of the ASTER data that was analyzed

Location	**Date taken**	**Time taken**	**Day/Night**
YPG #18688	4-26-2006	05:40:43 Zulu	Night
YPG #19184	9-22-2005	18:32:40 Zulu	Day
YPG #19170	10-1-2005	18:26:33 Zulu	Day
YPG#18678	10-1-2005	18:26:42 Zulu	Day
YPG #18686	11-18-2005	18:26:41 Zulu	Day
YPG #18681	11-18-2005	18:26:50 Zulu	Day

Table 8. ASTER level 1B data of Yuma Proving Grounds

Figures 12 thru 14 are the ASTER level 1B image chips that will be analyzed for the purpose of predicting helicopter brownout conditions. Level 1B data is defined as 1A data with radiometric and geometric coefficients applied. Level 1A data is image data plus radiometric and geometric coefficients. Data are separated by telescope.

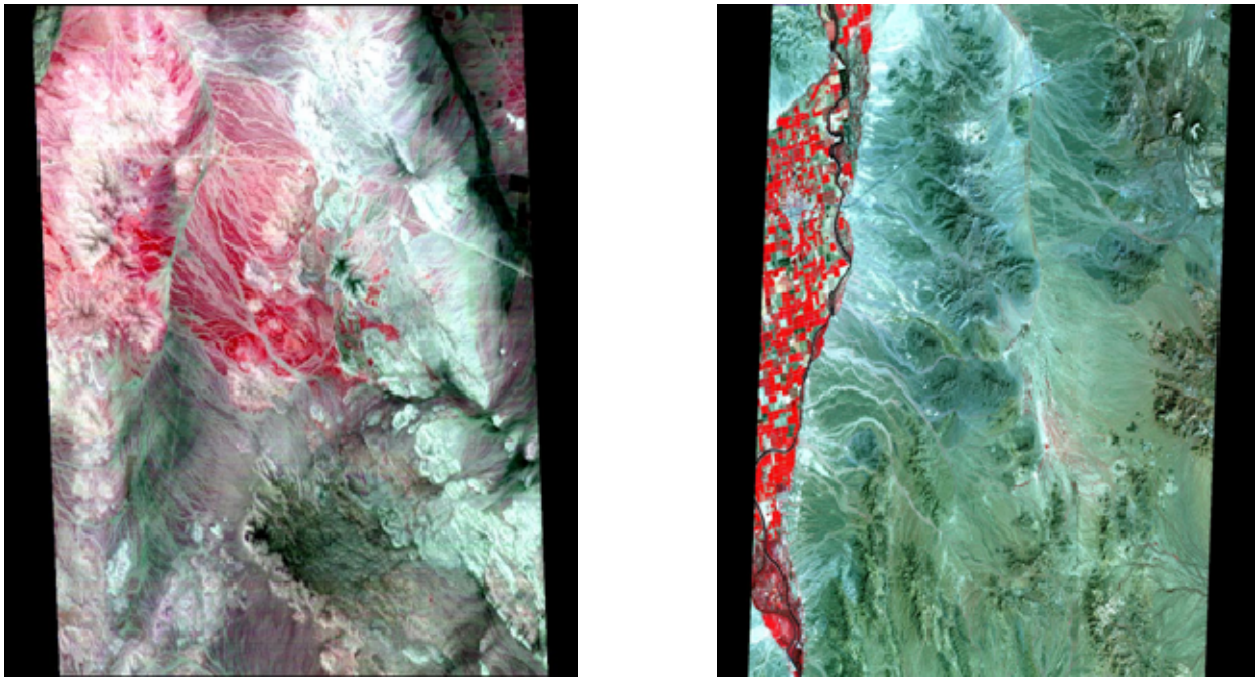

Figure 12. ASTER Level 1b data taken April 26 2006 at 0540 Zulu night time thermal (left) and September 22 2005 at 1832 Zulu daytime VNIR (right).

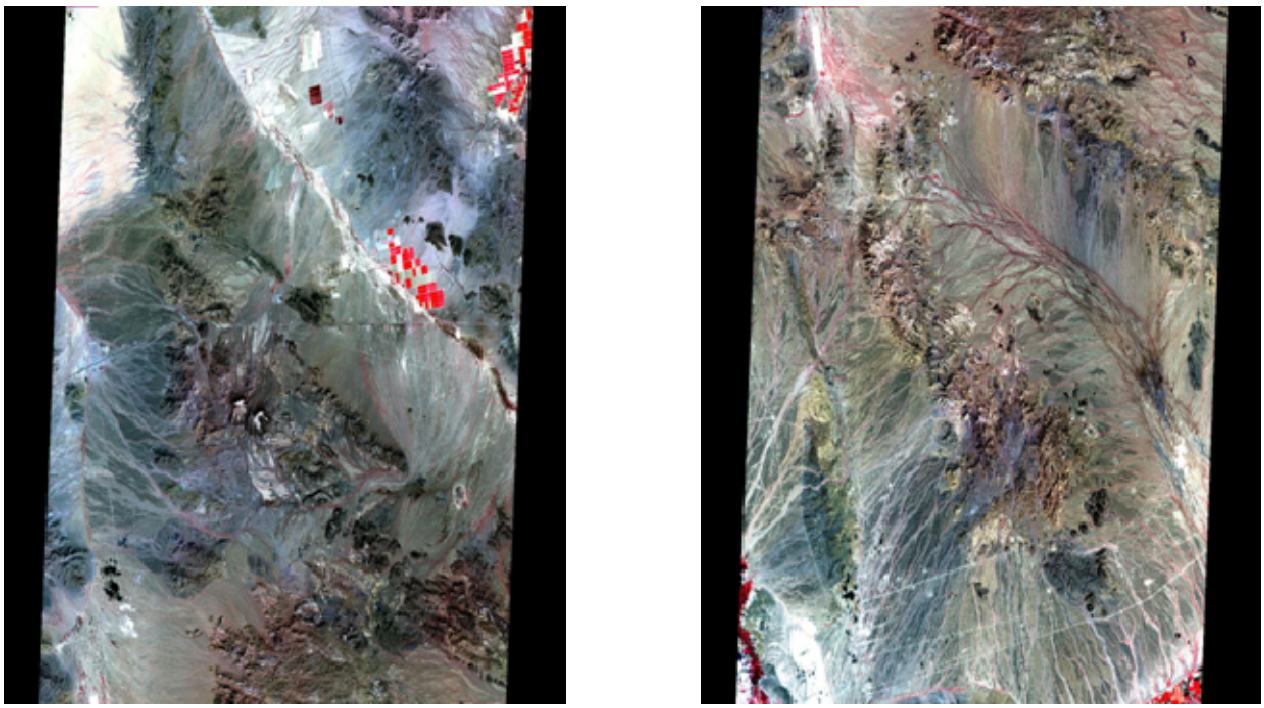

Figure 13. Level 1B data taken October 1 2005 at 18:26:33 Zulu daytime VNIR (left) and 18:26:42 Zulu daytime VNIR (right).

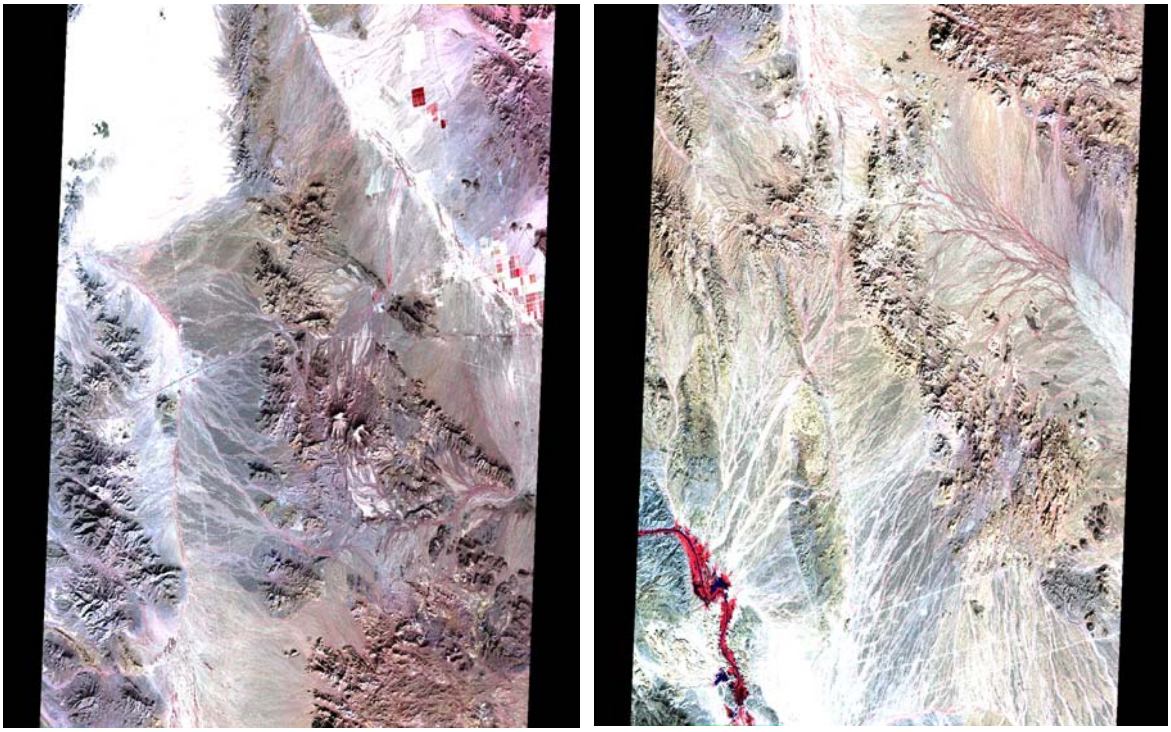

Figure 14. Level 1B data taken November 18 2005 at 18:26:41 Zulu daytime VNIR (left) and 18:26:50 Zulu daytime VNIR (right).

All ASTER data was prepared in the following manner. Images chips were combined into one image using the mosaicing function in the ENVI software. The image chip of YPG 19184 was set as the base image. Other images were registered to the base image.

b. Methodology

The ASTER data used for this thesis are the Visible Near Infrared (VNIR) and the Thermal Infrared (TIR) subsystems. The higher resolution VNIR data served as a base, the TIR data were resampled significantly to match.

c. NDVI

The NDVI values are the average of the difference between the Red and the NIR bands, essentially the slope from the Red to NIR. This is shown in a gray scale with brighter being more NIR reflective (greater chlorophyll) and darker representing a drop in reflectivity as the reflectance transitions into the NIR band. The following figures

show the difference in representation from the VNIR and NDVI. The NDVI values range from -1 to +1, and are conventionally adjusted to show a scale from 0 to 1. For the purposes of this thesis the range will remain in the negative to positive range. All figures have the same range scale shown for continuity and while it's a small range; any brighter or darker is not discernable without use of an imagery processing tool like ENVI or RemoteView. Figures 15 thru 17 below shows the original VNIR chips and its NDVI transform.

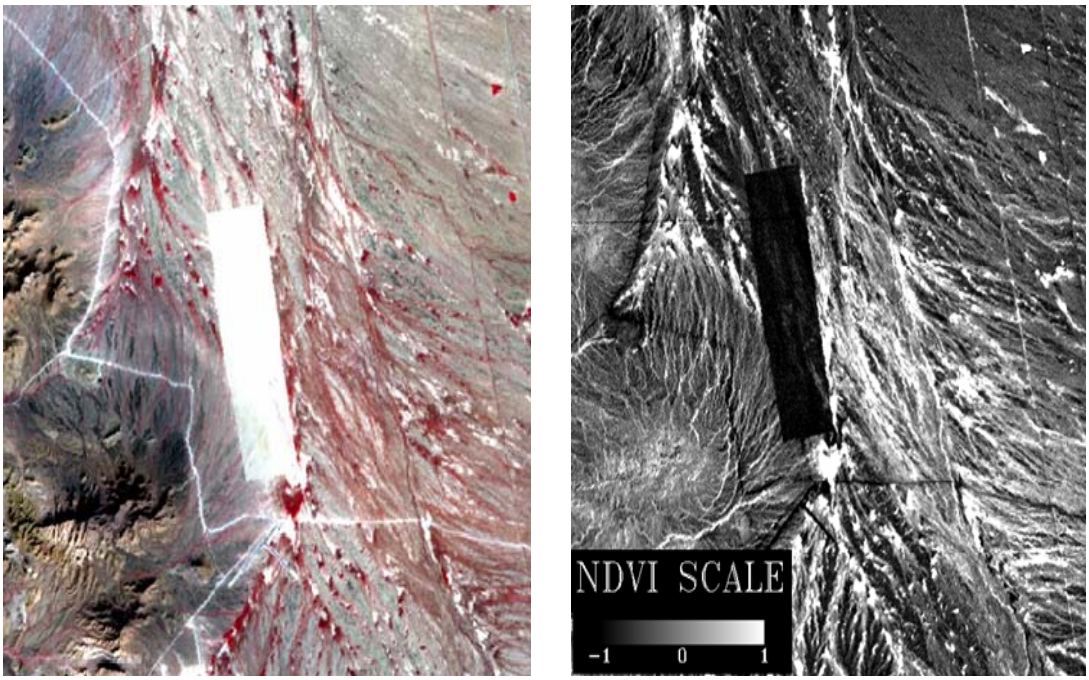

Figure 15. Visible Near Infrared and the associated NDVI transform for the granule ID # 18681_18688 taken at 18:26 Zulu on November 18 2005

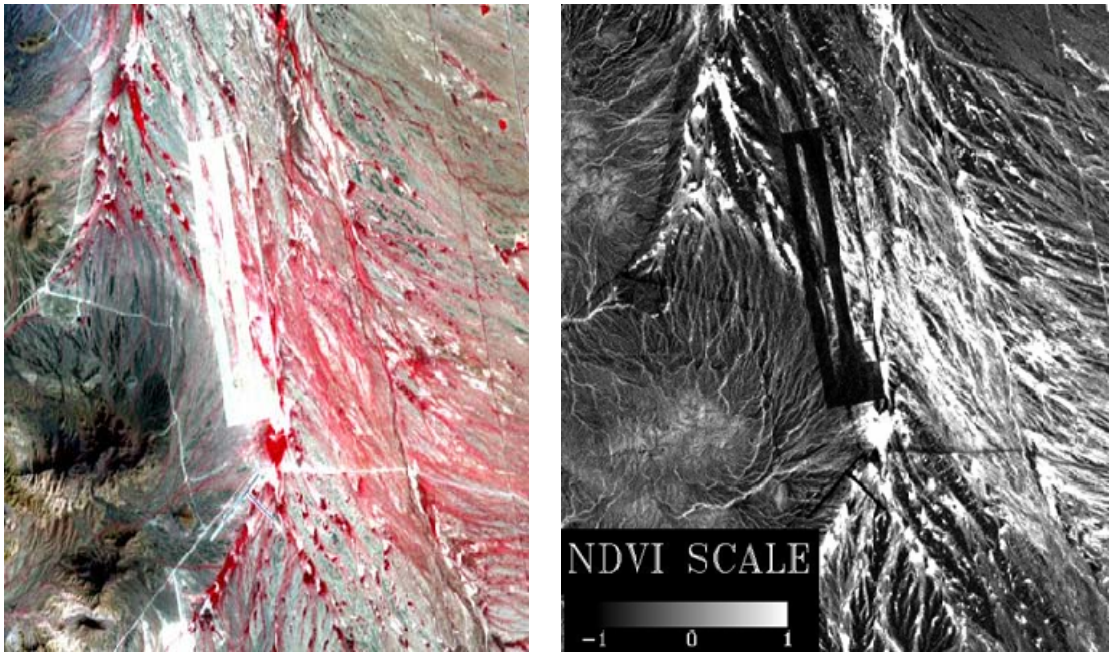

Figure 16. Visible Near Infrared and the associated NDVI transform for the granule ID # 19184 taken at 18:32 Zulu on September 22 2005

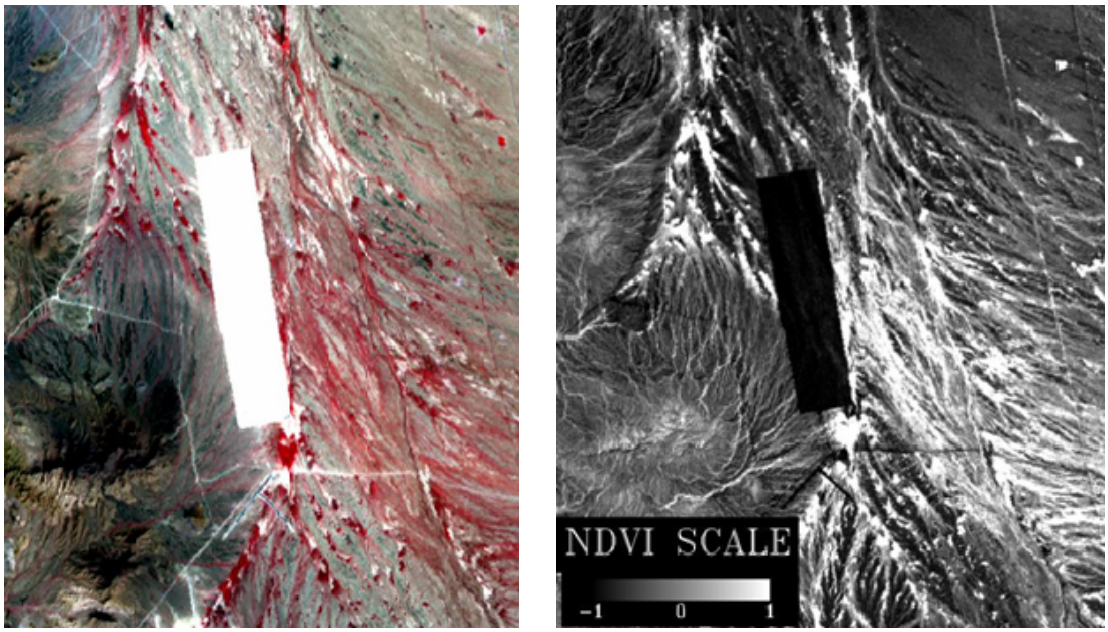

Figure 17. Visible Near Infrared and the associated NDVI transform for the granule ID # 19170_18678 taken at 18:26 Zulu on October 01 2005

d. Thermal IR

By comparing the thermal inertia of the various materials listed in the Table 4 soil with the lowest thermal inertia will cool the fastest and granite (mountain rock) will cool the slowest. The sandy gravel (desert pavement) will be close to the granite in the cooling rate and concurs with the slightly darker appearance of the non-brownout areas as compared to the brighter nearby mountains. Figures 18 and 19 shows the TIR images taken by ASTER of Yuma Proving Ground on the different dates from Table 4 The three highest thermal (LWIR) bands 14, 13, 12 were used in the RGB radio buttons in the ENVI software to best show the tilled field in the image. Temperature is a observed quantity while inertia is inferred. Inertia/change in temperature assumes some common start time/temperature.

Figure 18. ASTER Thermal infrared images of Yuma Proving Grounds Granule ID 19184 (left) taken September 22 2005 daytime thermal and 18681_18686 (right) taken November 18 2005 daytime thermal

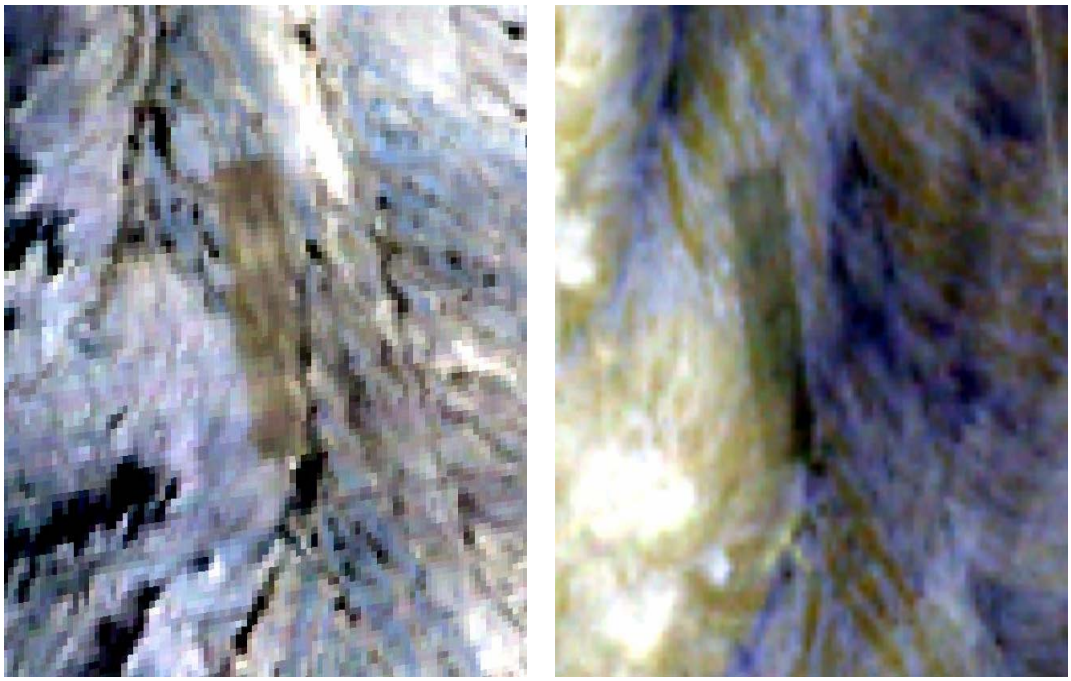

Figure 19. ASTER Thermal infrared images of Yuma Proving Grounds Granule ID 19170_18678 (left) taken October 01 2005 and 18688 (daytime) (right) taken April 26 2006 (night).

All Thermal IR (TIR) imagery has 90 meter resolution but the tilled field is visible in all image chips.

e. NDVI vs TIR Images, Scatter Plots and Histograms

In ENVI, Scatter plots can be used to display two (or three) image bands in a plot window. From this plot, and some knowledge of spectral signatures, one can determine the general cover types as well as their location within the image. When working with scatter plots we describe this as working in *spectral space* as opposed to the *image space* when using the imagery directly. Scatter plots provide a good way to show the relationship between *spectral* and *image space*.

The ASTER data with granular ID # 18681_18686 taken November 18 2005 will be used to show the NDVI vs TIR image chips and their associated 2D scatter

plots. For the first set of data that is analyzed the two bands that are used for the scatter plots are the NDVI and the highest band (band 14) within the thermal band that will build the scatter plot.

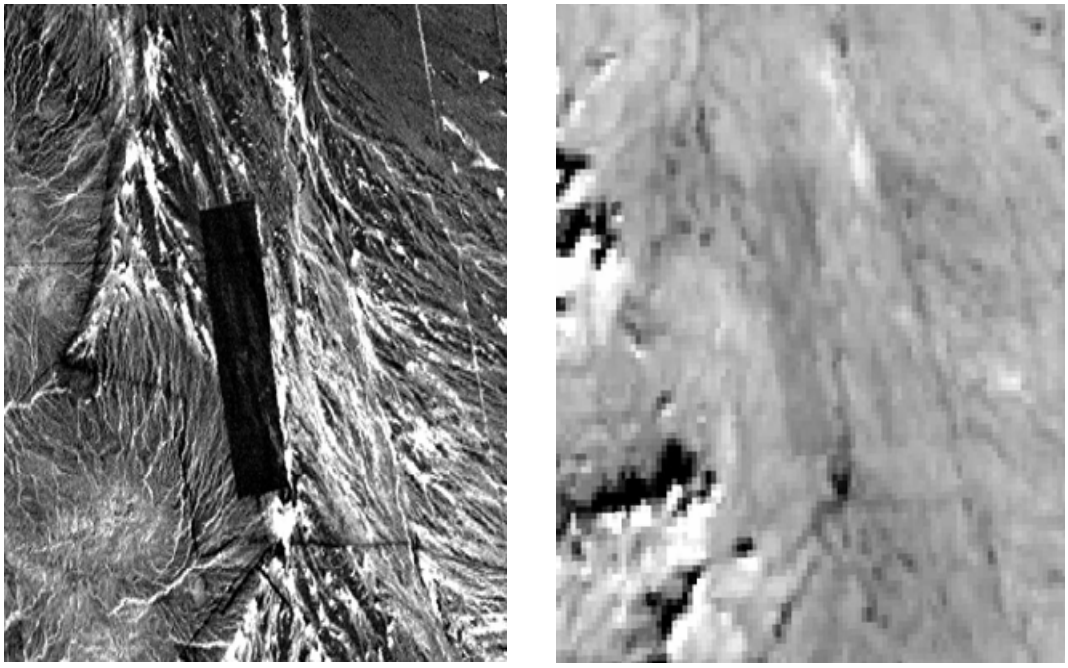

Figure 20. NDVI (left) and thermal band 14 (right) daytime of ASTER data taken November 18 2005.

Figure 20 shows the NDVI and Thermal images that are used to create the scatter plot. NDVI is used for the x axis and the TIR (band 14) is used for the y axis. These two bands yield a scatter plot return shown in Figure 21.

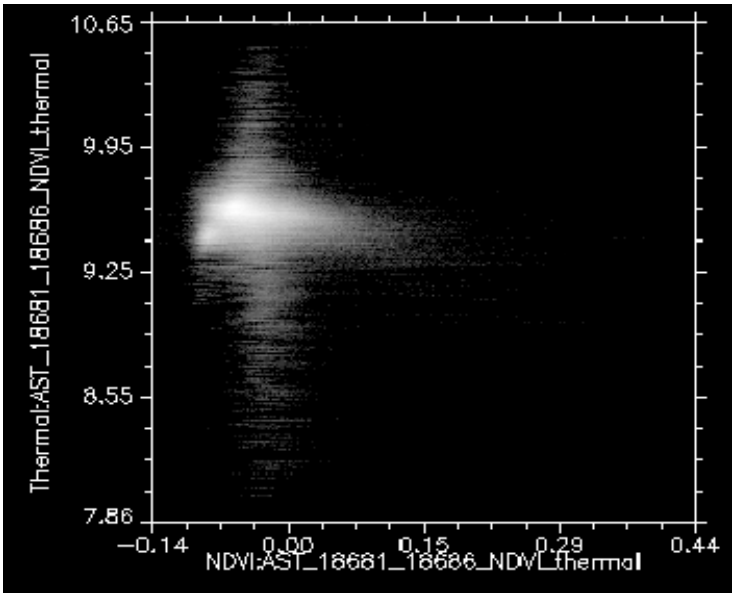

Figure 21. NDVI versus Thermal Infrared 2D scatter plot of November 18 2005 data

At first glance the scatter plot looks rather uniform for the given picture; however, a closer assessment revealed a pixel cluster on the left of the 0.00 point and slightly above 9.25 on the y axis Figure 22 shows the location of the pixel cluster.

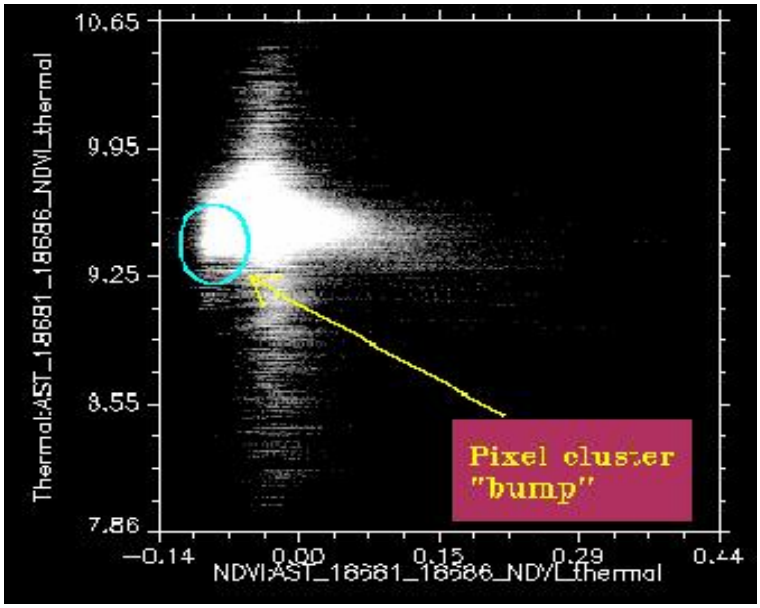

Figure 22. November 18 2005 NDVI vs Thermal 2D scatter plot illustrating pixel cluster.

It was stated earlier in this thesis that darker regions in NDVI represented areas with scarce vegetation while brighter areas represented areas with healthy vegetation. Also in thermal images darker areas represented regions within the image that did not have a high thermal inertia such as sand and soils whose thermal inertia is (0.024) from Table 7 and brighter areas represent regions with a moderate or high thermal inertia such as that of vegetation (0.036) and granite (0.054). Knowing this one can say darker regions represents bad landing zones and brighter areas represent good landing zones.

During the analysis of the pixel cluster, it was observed that the pixel cluster represented the tilled field in the image. This led to the designation of labeling the first region of interest in red representing the tilled field or bad landing zone. By doing this and coloring the entire pixel cluster red yielded interesting results as shown in Figure 23.

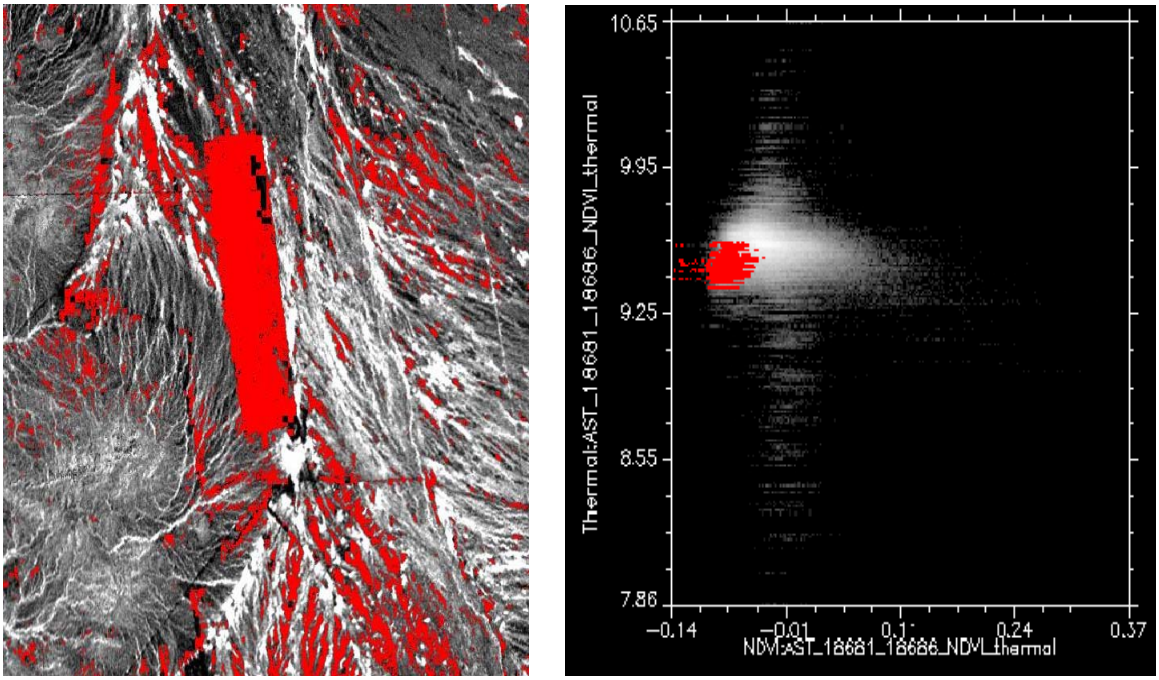

Figure 23. NDVI with red (tilled field) region of interest (left) 2D scatter plot with pixel cluster colored as red ROI.

It is observed in the above illustration by marking the pixel cluster in the scatter plot as a red region of interest also marks the majority of the dark regions (bad landing zones) as red also in the NDVI vs Thermal images. Figure 24 shows results on the thermal image.

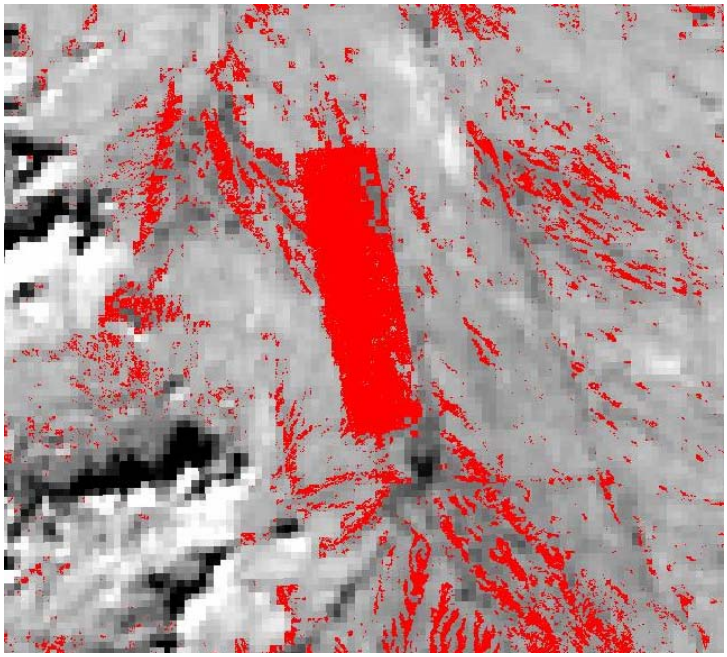

Figure 24. Thermal Infrared November 18th image with red (tilled field) region of interest.

The next challenge is to see if the NDVI vs Thermal scatter plot can tell where the good landing zones are within the image. Using the same basic technique as described above it was discovered that the majority of the heavily vegetated areas resided in the far right quadrant of the scatter plot and is illustrated in Figure 25 below.

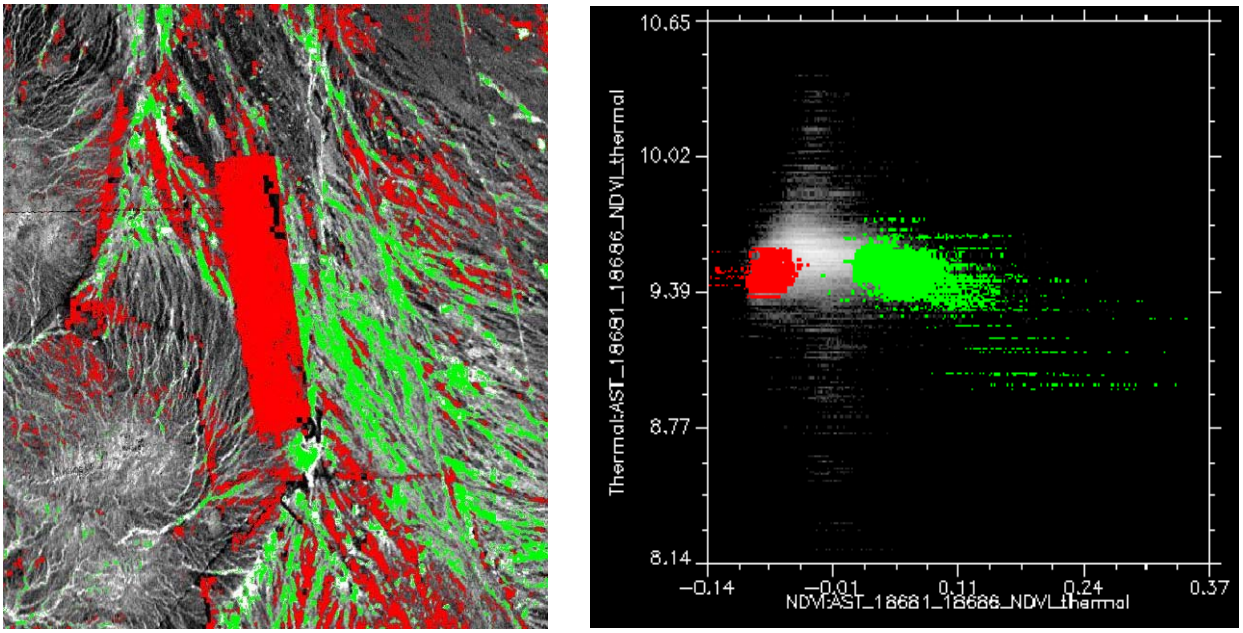

Figure 25. NDVI with red ROI (tilled field/silt) and green ROI (vegetation area) (left) and 2D scatter plot with red and green ROIs.

All other regions that are not red (bad landing zone) or green (good landing zone) were labeled as a blue region of interest (ROI) where within the image the training area appeared grey Figure 31 shows the resulting image and scatter plot.

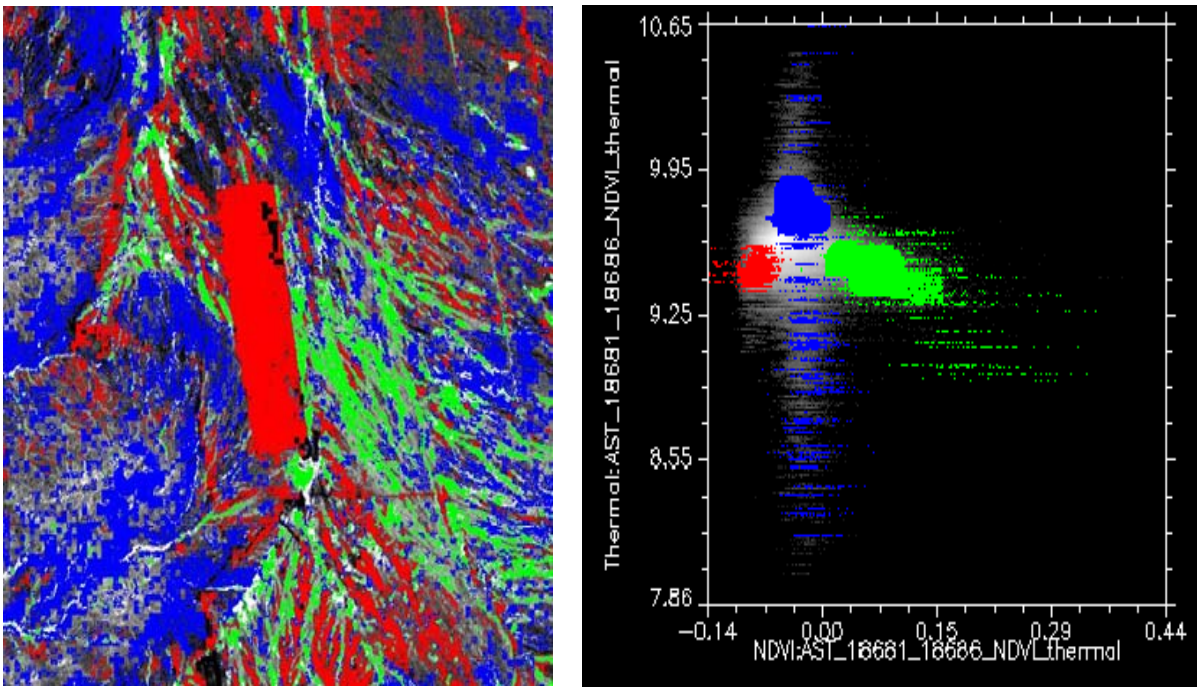

Figure 26. NDVI image of November 18 2005 data with all associated regions of interest

The image in Figure 26 resulted in the following histograms shown in Figure 27 and 28. Histograms are the graphical display of the tabulated frequencies in the image of different bands in this case the NDVI and the thermal band.

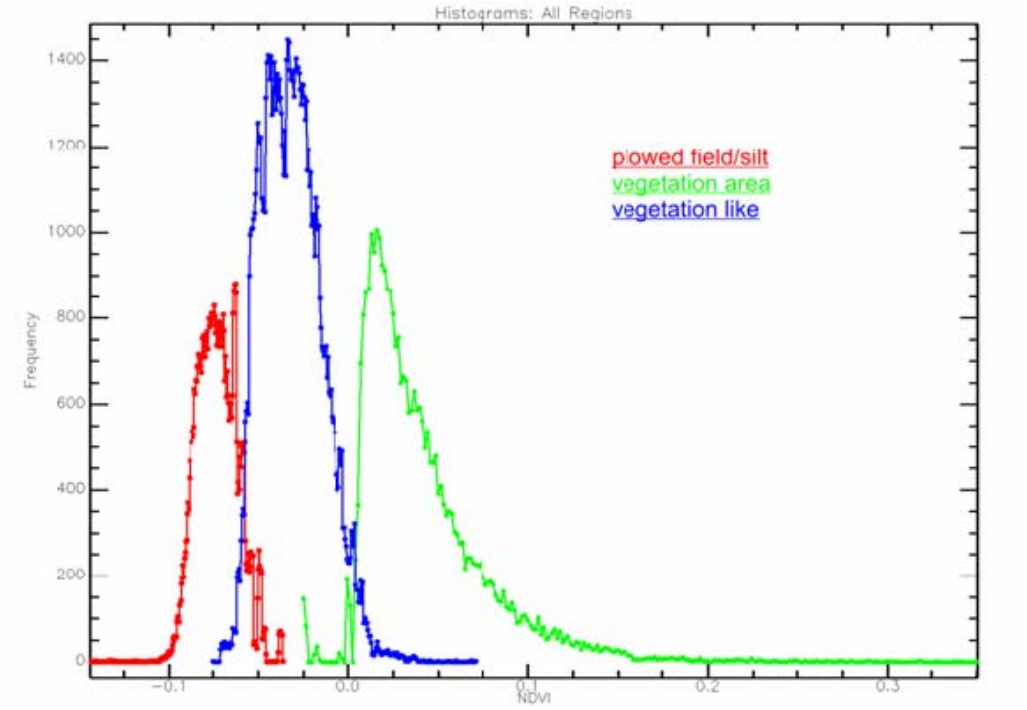

Figure 27. NDVI band histogram from November 18 2005 image regions of interest

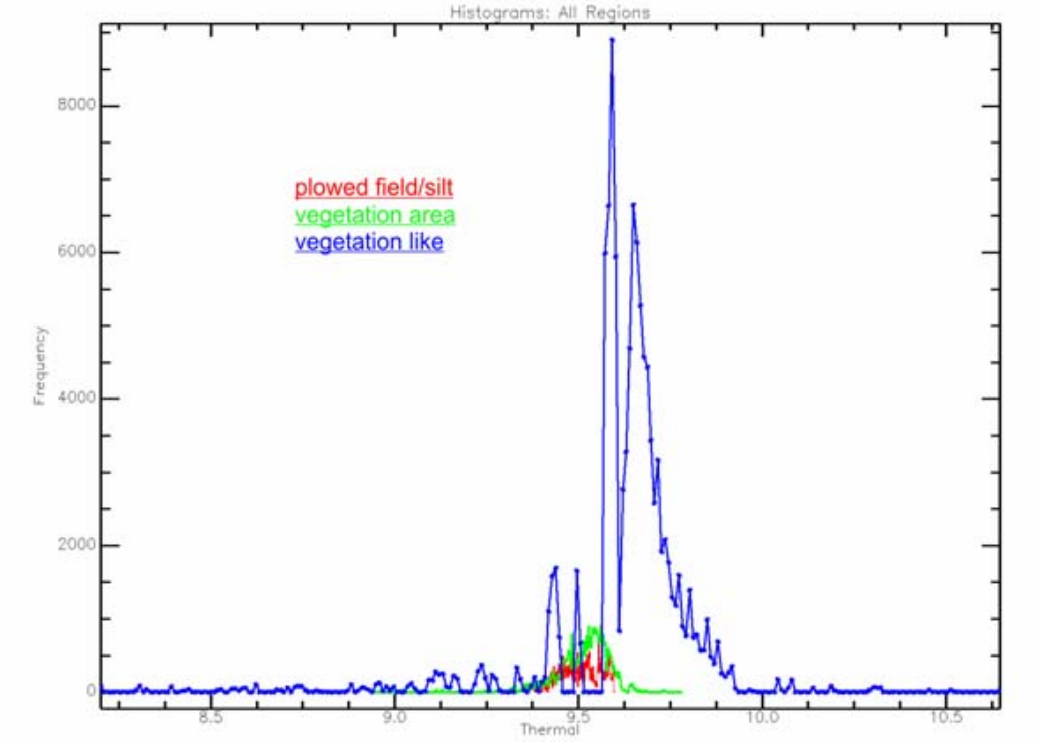

Figure 28. Thermal band 14 histogram from November 18 2005 image region of interest.

The resulting Regions of interest were inputted from the 2D scatter plot into the Maximum likelihood analyzer to reprocess the image. The Maximum likelihood classifier uses the distribution of data within each ROI to calculate n-D probability functions for each class. Each pixel is assigned to the class for which the highest probability is calculated. This classification works best when the data is normally distributed as in the above image. Figure 29 shows the resulting class image.

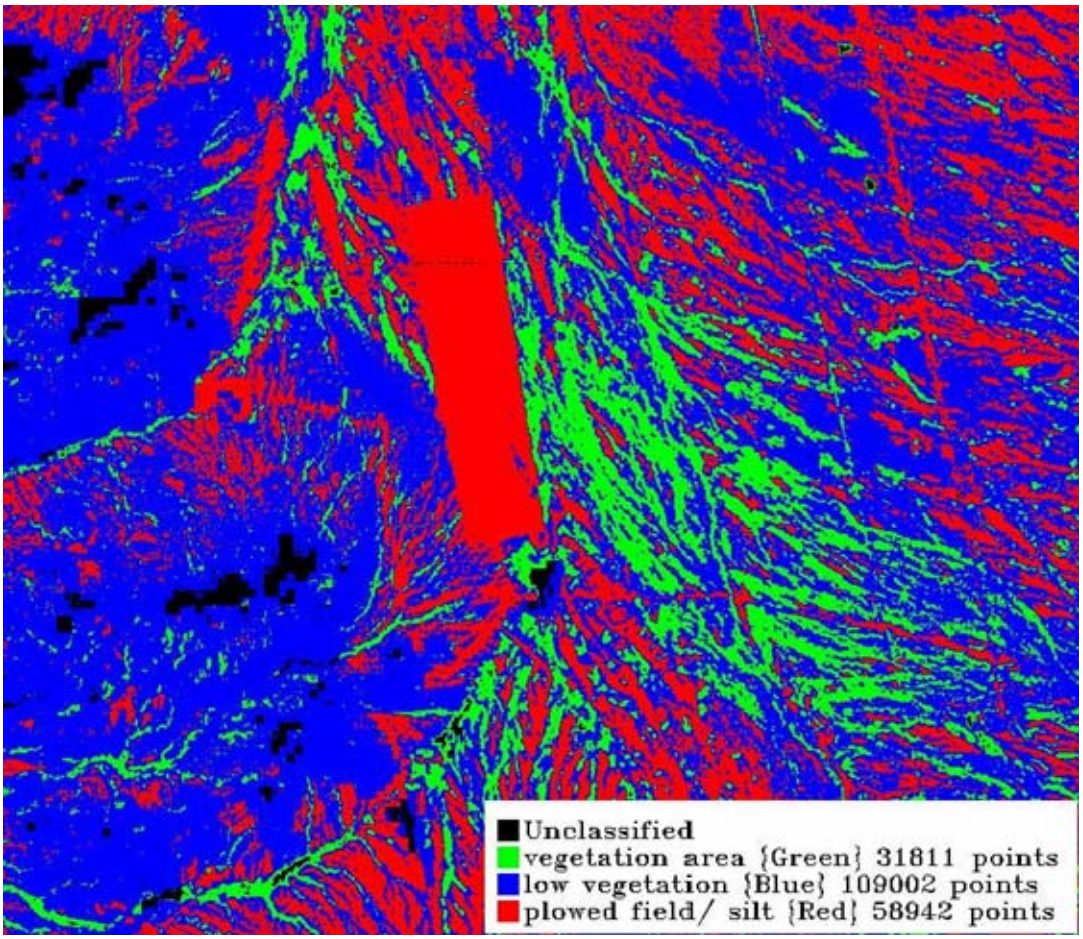

Figure 29. Maximum likelihood classified image of November 18 2005 image.

Figure 29 shows the ability to classify the entire scene. This shows which areas have the probability of being bad landing zones and which are good and average respectively. The maximum likelihood classifier was used with 95% probability was used in the initial parameters. The unclassified areas are the results of using that 95%. This

image was taken November 18 2005 which according to Table 6 is a daytime image taken at 18:26:41 Zulu. This analysis was done using NDVI and the thermal band. The next question that must be asked is can a image be created if only one of the bands are available for use? This question can be answered using the minimum distance classifier function in ENVI which calculates the distance of each pixel in n-D spectral space from the n-D means ROI where n is the number of bands. The pixel is assigned to the class corresponding to the ROI with the closest mean. If the pixel is beyond a threshold distance from the closest mean, it remains unclassified. Figure 30 shows the minimum distance classified image of the NDVI band of the November 18 2005 image

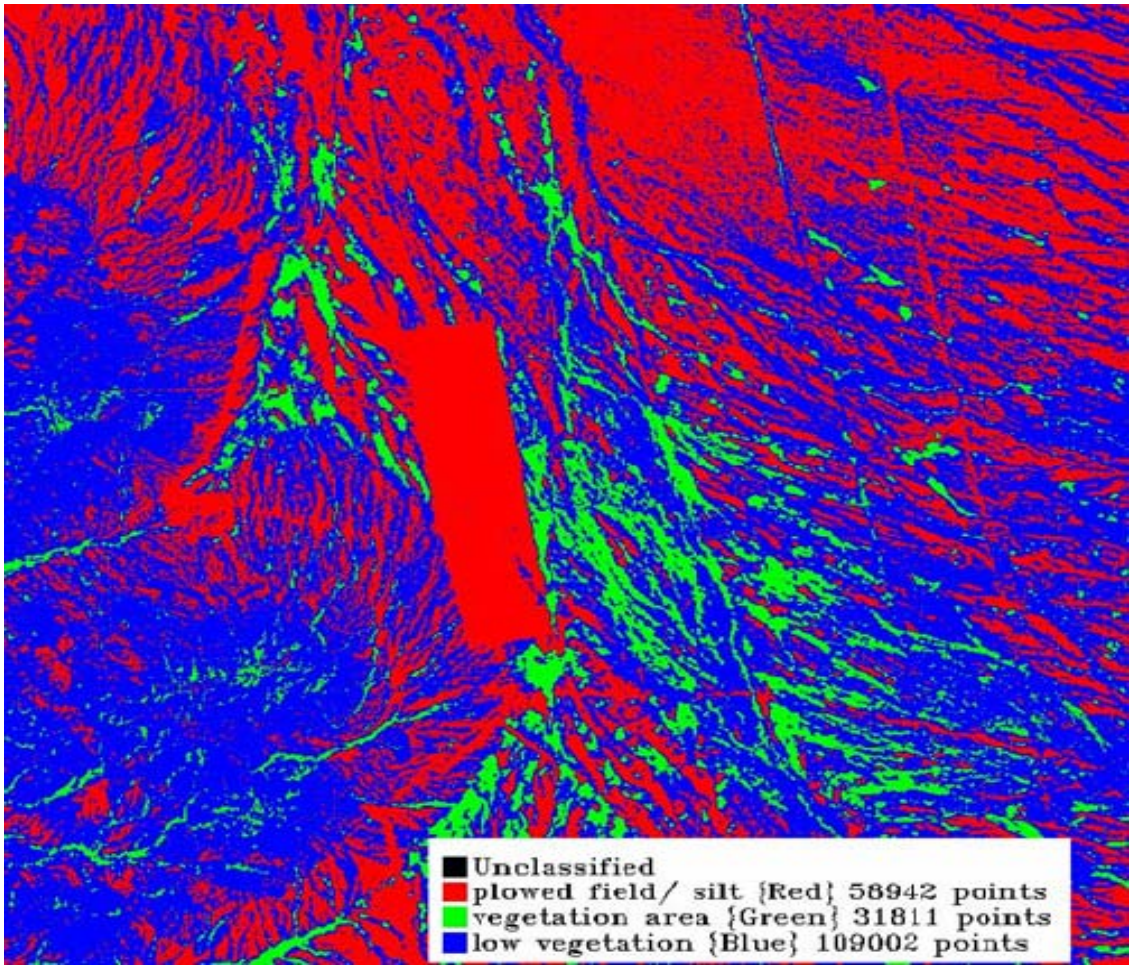

Figure 30. Minimum distance classified NDVI band image of November 18 2005 image.

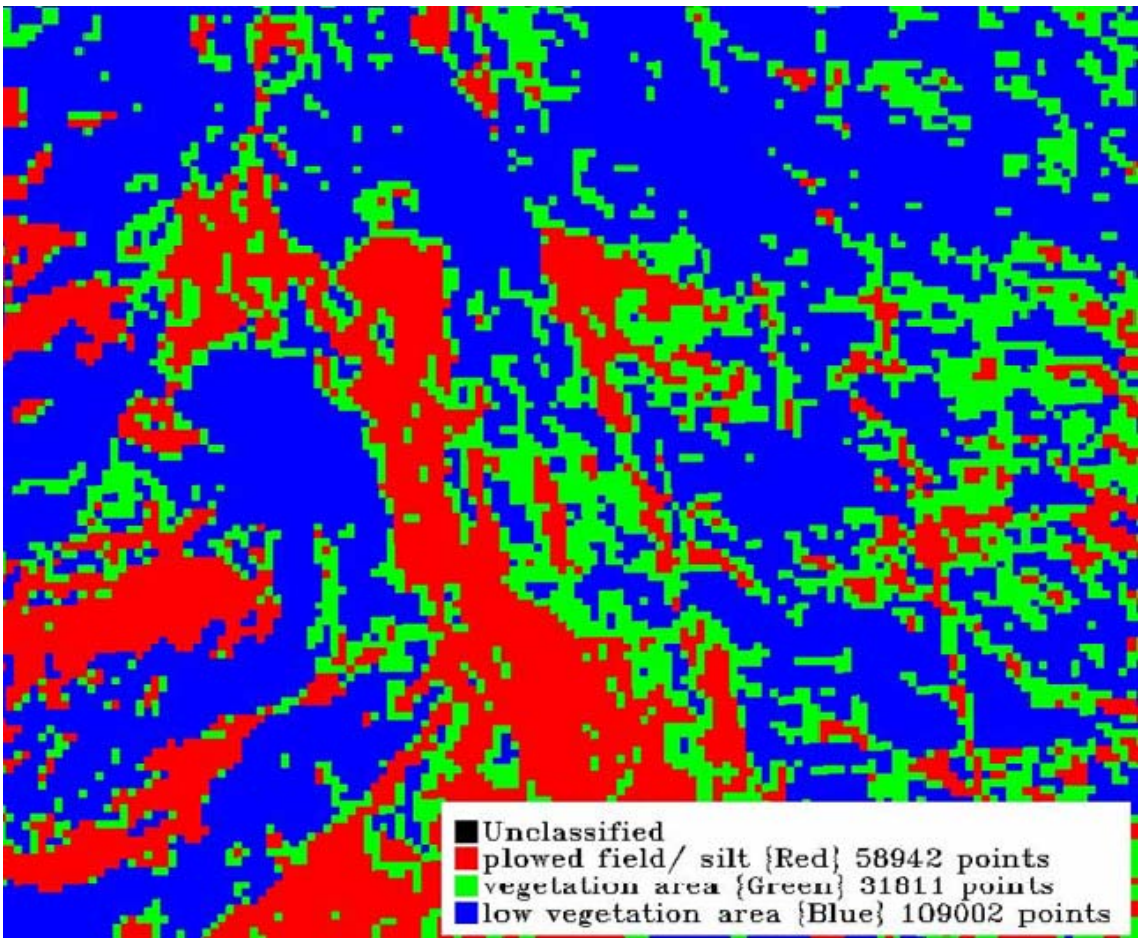

Figure 31. Minimum distance classified image of the thermal band of the November 18 2005 image.

The season and the time must be taken into consideration because these factors may effect the outcome when classifying the image due to environmental changes therefore other images were taken at different times and dates using the same technique as above to show that ASTER data can be used at any time and date to predict a possible brownout condition could exist and is illustrated in the following figures.

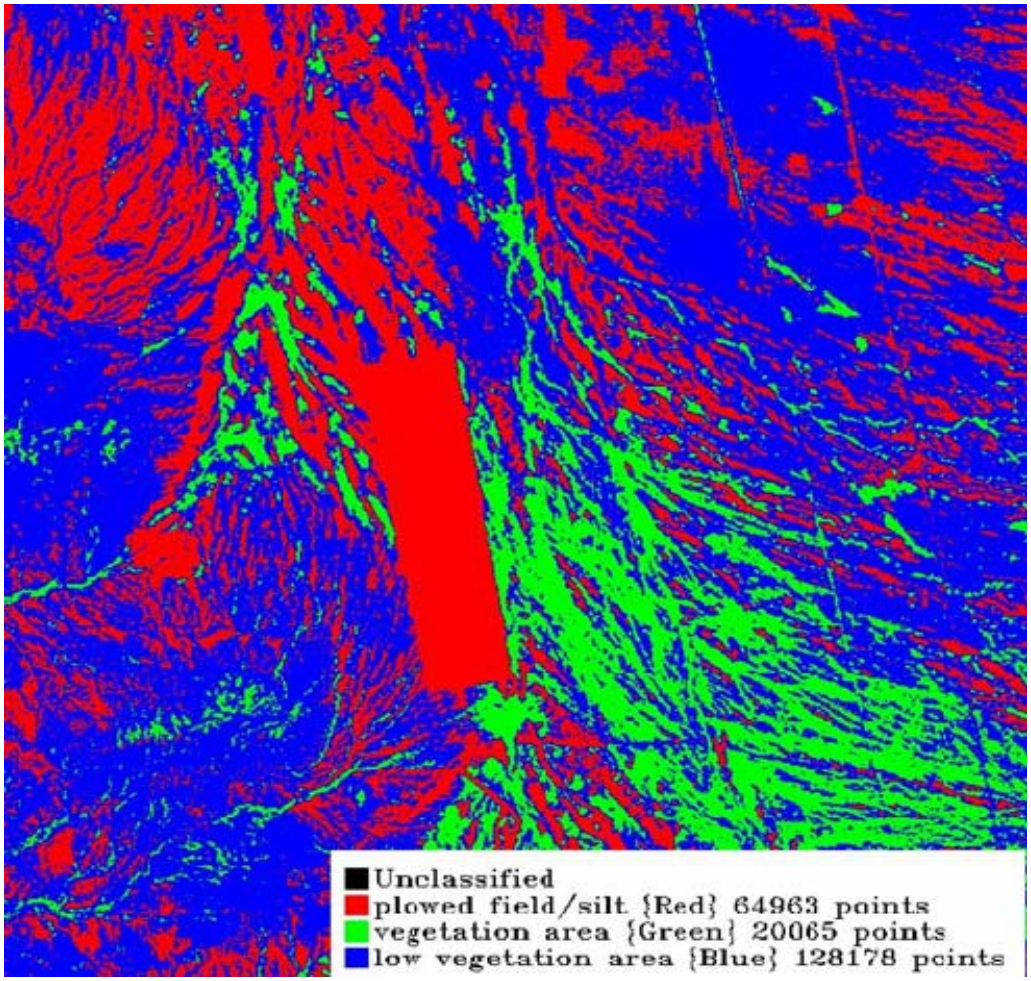

Figure 32. Maximum likelihood classified image of the NDVI vs Thermal ROIs of the October 1 2005 data set.

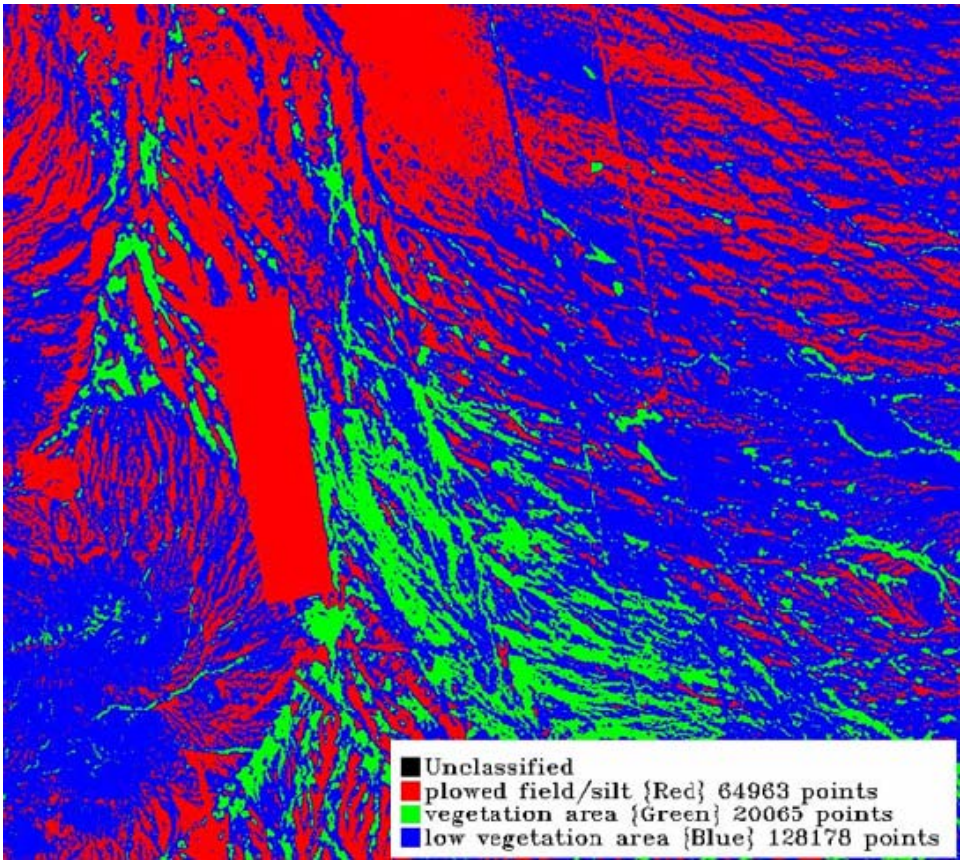

Figure 33. Minimum Distance classified image of the NDVI band ROIs of October 1 2005 data

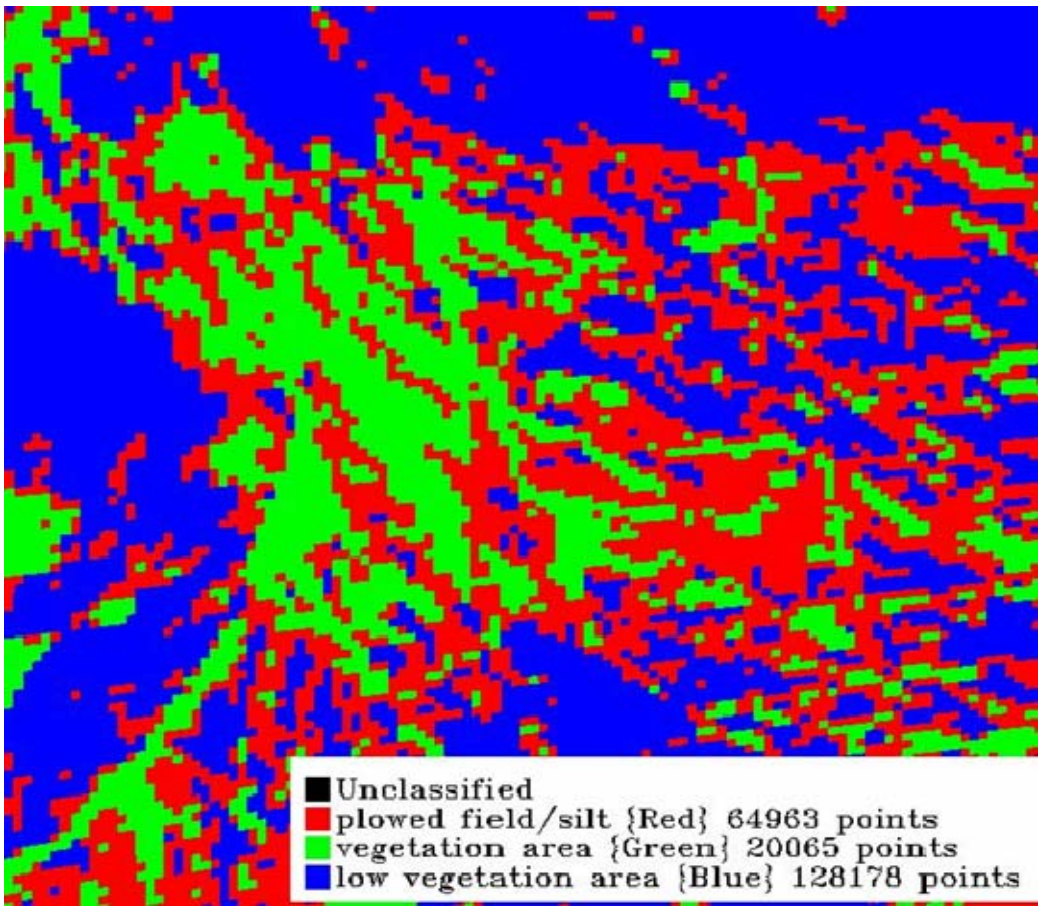

Figure 34. Minimum Distance classified image of the thermal band ROIs of October 1 2005 data.

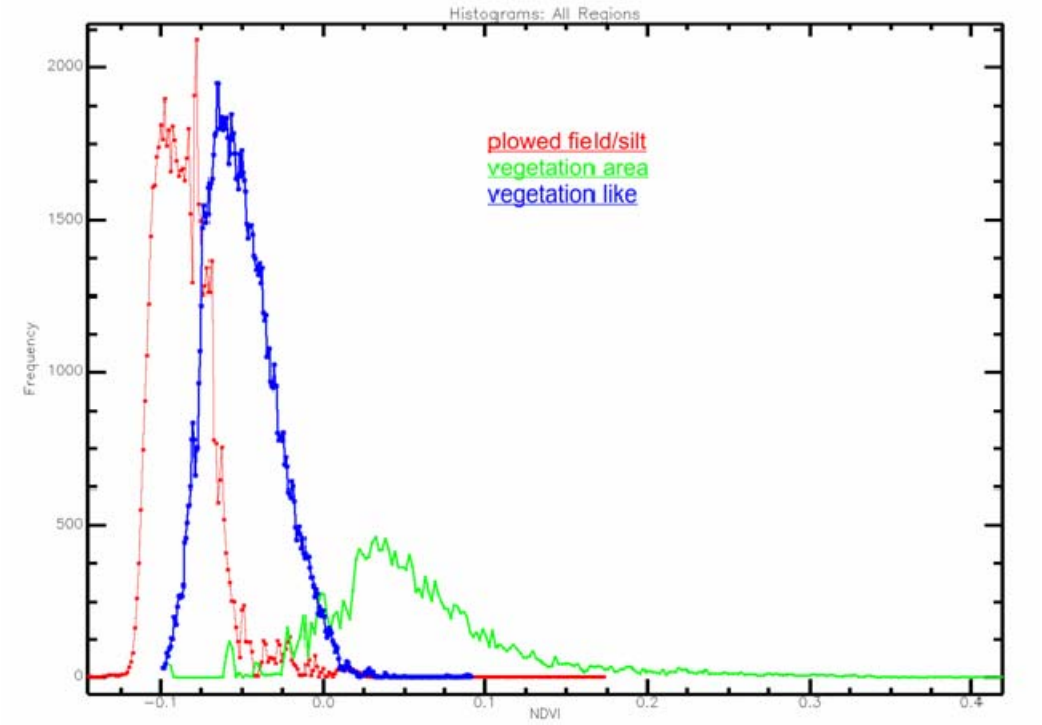

Figure 35. NDVI band histogram from October 1 2005 image regions of interest

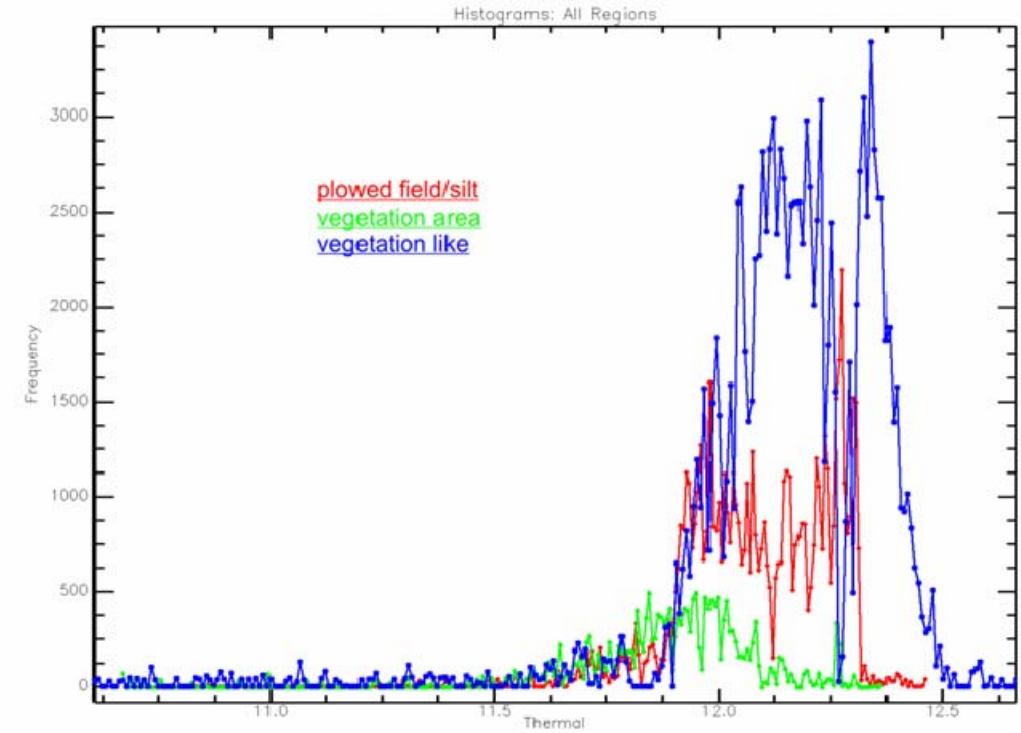

Figure 36. Thermal band 14 histogram for October 1 2005 data.

Note that in Figure 34 the plowed field is not visible which may be due to the resolution or due to some environmental factor.

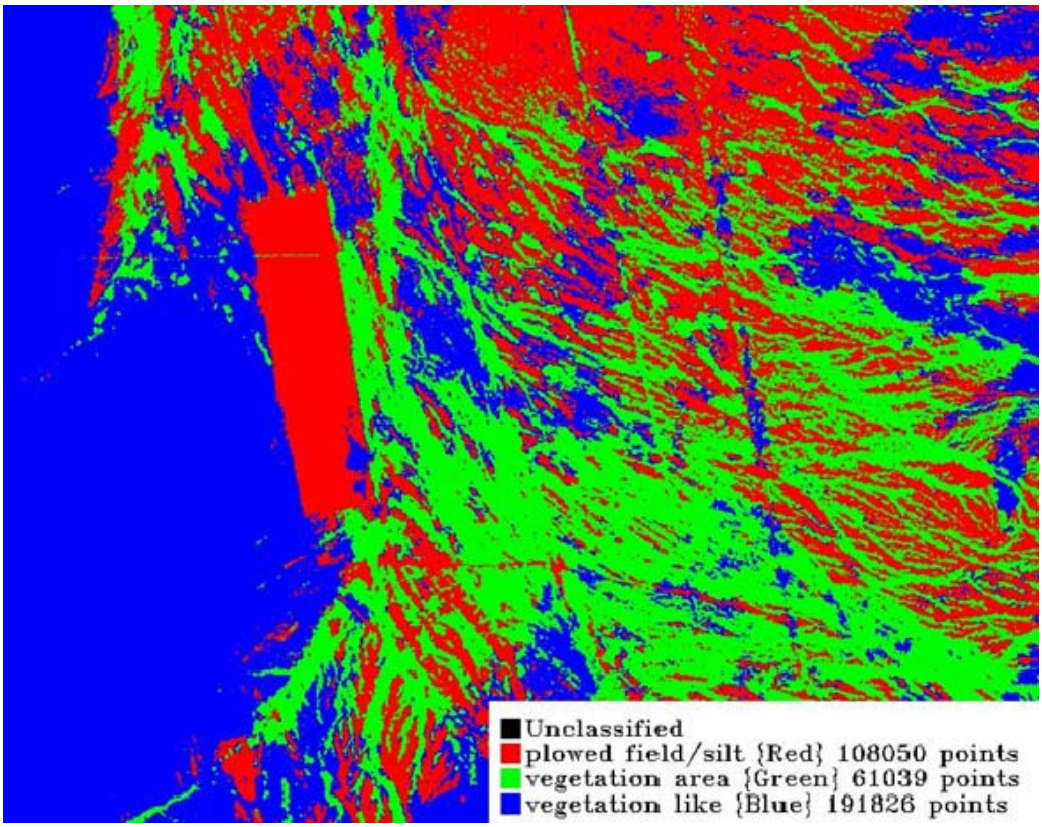

Figure 37. Maximum likelihood classified image of the NDVI vs Thermal ROIs of the November 18 2005 and April 26 2006 nighttime thermal data.

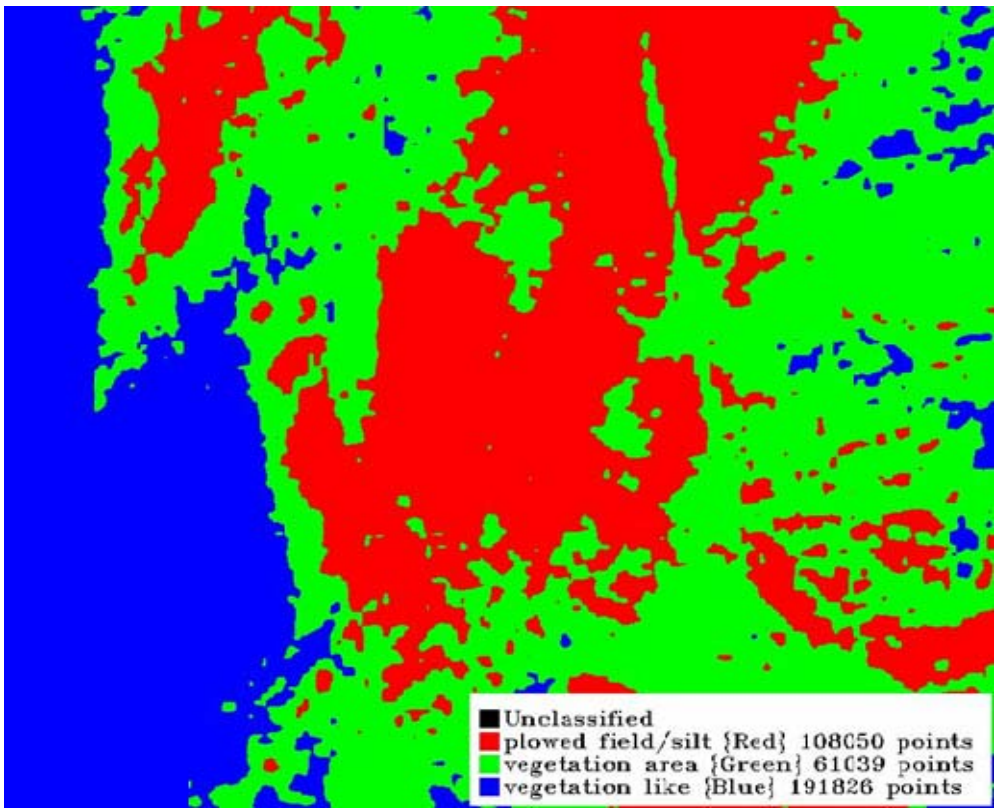

Figure 38. Minimum Distance classified image of the thermal band ROIs of April 26 2006 data.

Figure 38 shows the classified image of the thermal band of the April 26 2006 data which is the only nighttime thermal imagery taken of YPG from ASTER. It had to be combined with the November 18 2005 daytime visible. The plowed field can still be detected in the above figure to some degree.

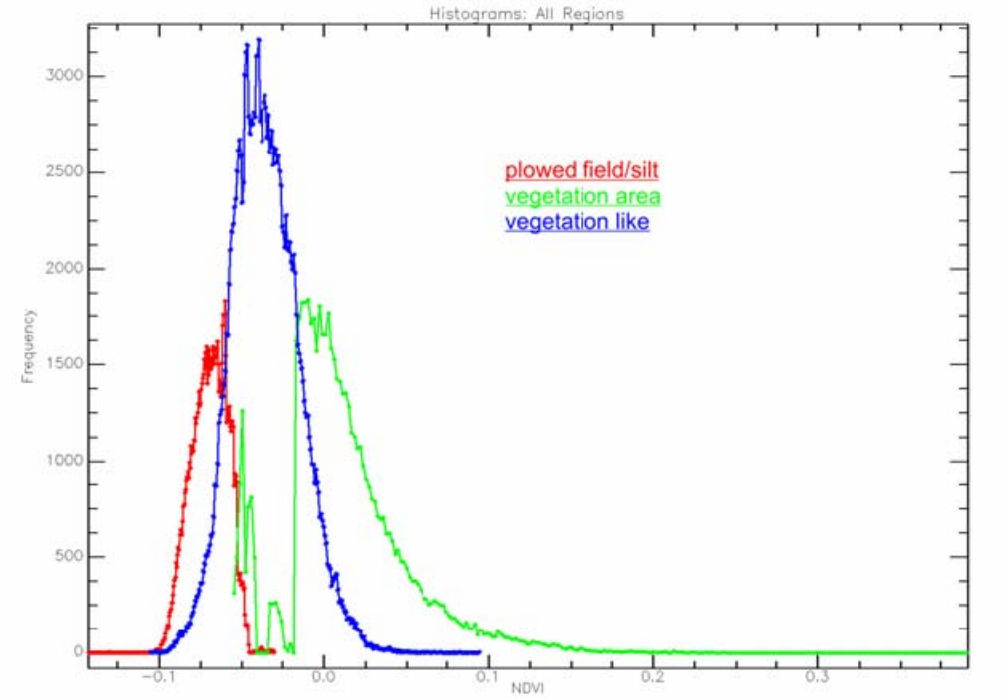

Figure 39. NDVI band histogram of April 26 2006 image.

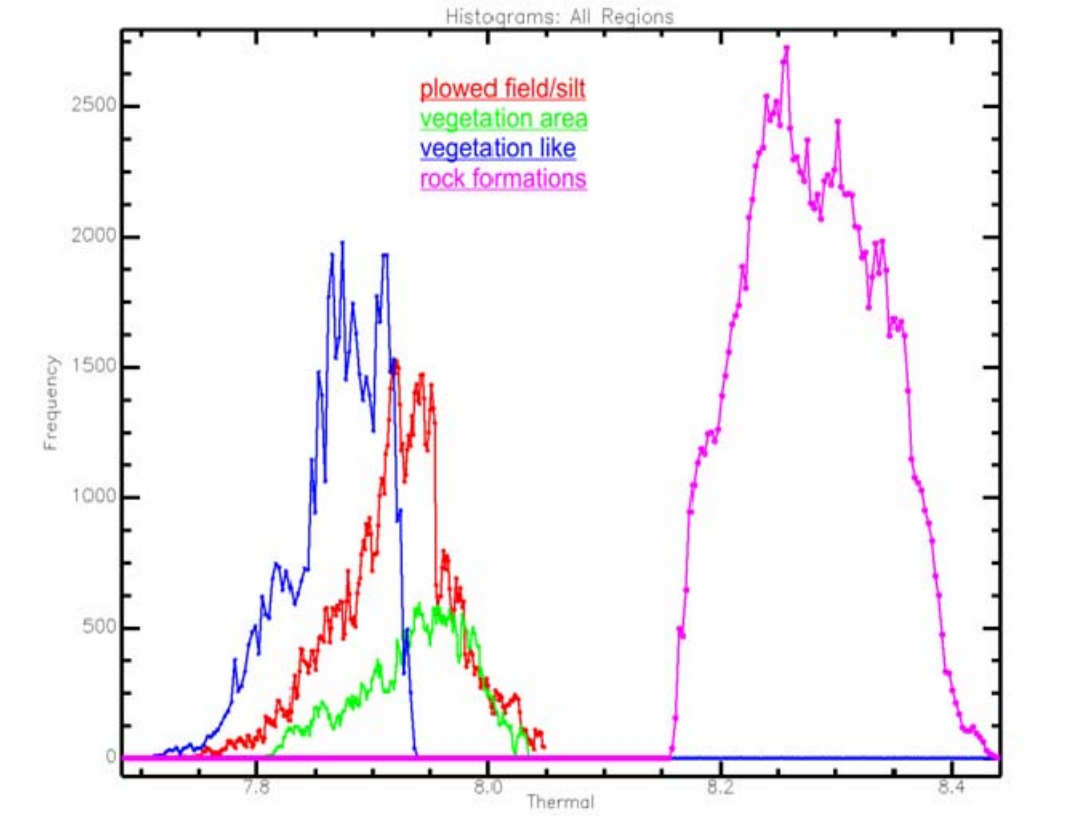

Figure 40. Thermal band 14 histogram of April 26 2006 data (Night)

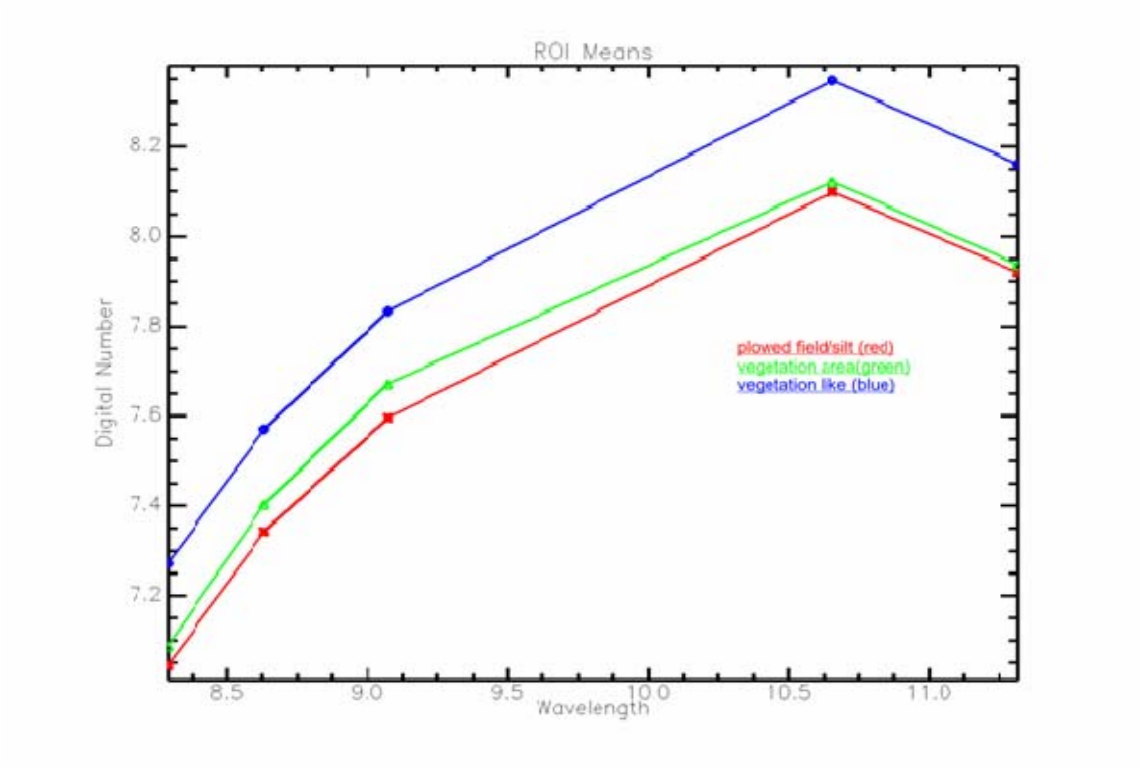

Figure 41. Thermal IR bands ROI means graph of night data

f. Image Analysis Results vs Ground Truth

Now that a technique has been established that is consistent throughout all of the images it must be compared to the ground truth. Major Michael Shewfelt's iteration of the BOA thesis had established ground truths for the YPG area. A site visit was made to the Yuma Proving Grounds on 7 July 06 to revisit the site previously observed during DARPA funded brownout testing. The site of the testing was located at: Lat/Long N33˚ 23.764'/ W114˚ 16.575'. This was the center of a 1000 meter square area of tilled soil. To the north of the LZ, 1000 meters, was a gravel area that appeared to be a good LZ and had no dust stirred up from the vehicle traffic. This LZ was centered at Lat/Long N33˚ 24.025'/ W114˚ 16.754'. The area surrounding the tilled LZ test area had brush like vegetation and a crust of soil 1 to 2 inches deep, which once broken allowed the soft silt underneath to be blown up into the air.

The extremely bad section of the LZ that was previously tested was bisected by the N-S road and ran adjacent and parallel to the E-W road. The center mark

listed above (Lat/Long N33˚ 23.764'/ W114˚ 16.575') is located in the SE quadrant of the area divided by the intersection. The SE and SW quadrants have the same texture and composition with a ¼ to ½ inch crust that is easily broken and exhibits the same brownout soils as were blown up by the helicopter in the March test. The good LZ (Lat/Long N33˚ 24.025' / W114˚ 16.754') with gravel and solid crust was still evident this time and remained undisturbed. It is located in the NW quadrant of the area.

Figure 42 below shows the good and bad landing zones labeled on the November 18 2005 max class data. The coordinates that were given by Major Shewfelt in his Yuma trip report both fall in the Regions of Interests that built the maximum classified image red (bad landing zone) and blue(low vegetation area). This shows that the ASTER data can be used to help accurately predict a helicopter brownout condition.

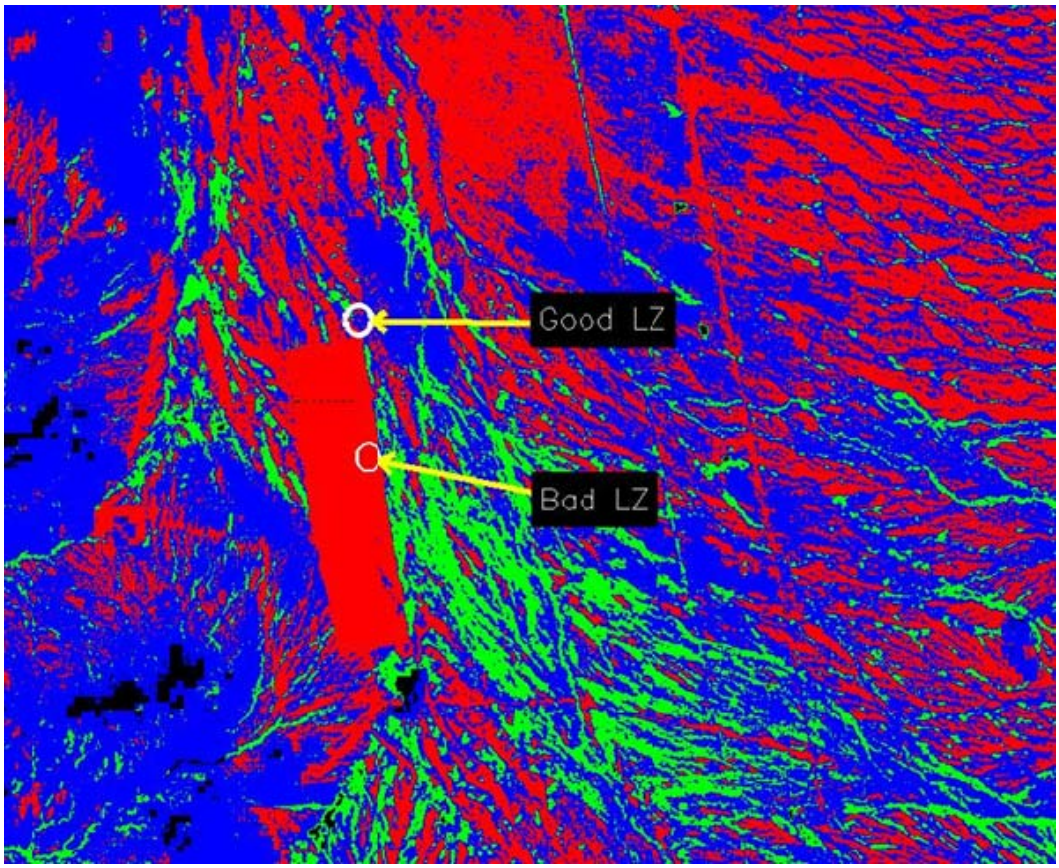

Figure 42. Maximum Likelihood Classified image of November 18 2005 data with the good and bad landing zones labeled.

2. Iraq Imagery Analysis

Iraq imagery data was taken by the QuickBird satellite only. There are no Infrared images of Iraq to use the 2D scatter plot technique that was used for Yuma Proving Ground. However, the NDVI transform can still be used in the analysis of the Iraq data and given what is know about how NDVI is used in vegetation analysis brownout probability can still be predicted using just the NDVI band.

Location	Date
Abu_Dhakar	28 September 2006
Ar_Rutbah	22 July 2004
Al_Asad	15 September 2006
Rawah	16 October 2006
Al_Qaim	28 November 04
Anah	06 October 2006

Table 9. Locations and dates of MSI data taken of Iraq.

.

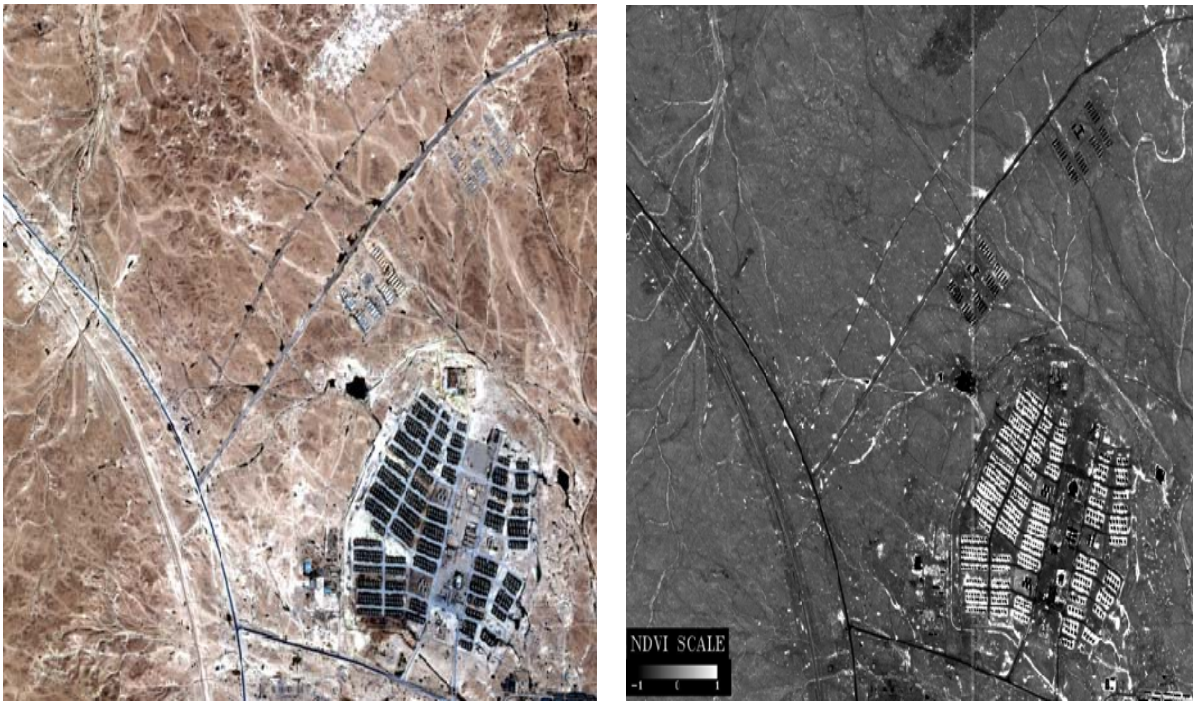

Figure 43. QuickBird MSI Image of Al-Asad taken 19 April 2006 and its NDVI transform.

Using the technique that was used for Yuma Proving ground will not work due to there are not thermal images available to apply the 2D scatter plot technique. However, MSI data for the areas yields an associated NDVI transform that by itself can be used to help predict possible brownout conditions in that area.

The Al-Asad image is used as the model for the following technique. Within the NDVI image of Al-Asad training areas were selected for Regions of Interest red (bad landing zone area) where areas in the NDVI image that appeared dark or black in the image. Blue regions of interest (low vegetation area) depict some vegetation and appear grey in the NDVI image. The green regions of interest were used to show where healthy vegetation was in the NDVI image. Figure 43 shows the Al-Asad NDVI image with the region of interests.

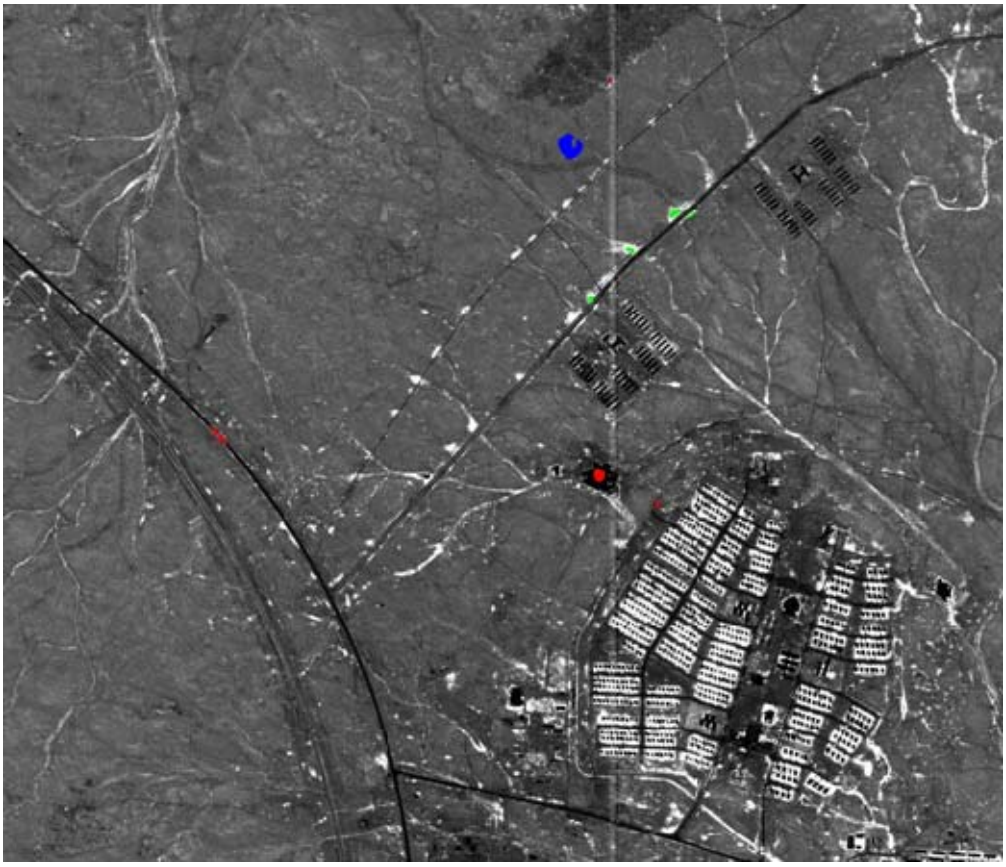

Figure 44. Al-Asad NDVI image with Regions of interests (ROIs).

Figure 44 shows the NDVI image with the associated regions of interest. These regions of interest were then entered into the minimum distance classifier with the NDVI band. Figure 45 shows the resulting minimum distance image from Figure 44's ROI's.

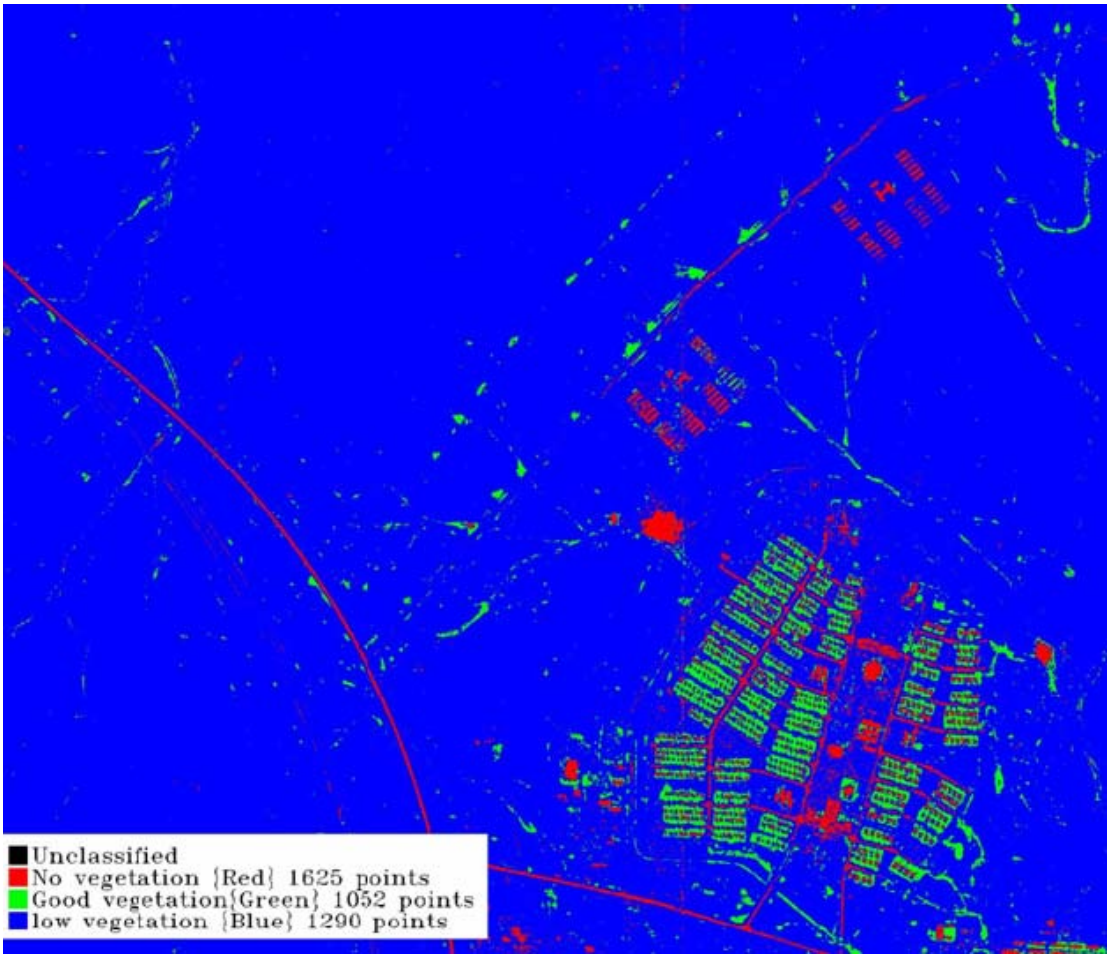

Figure 45. Minimum distance classified image of Al-Asad.

Figure 45 shows the areas that are possibly bad landing zones in red (no vegetation) and the possible good landing zones in blue (low vegetation) and green (good vegetation. Figures 46 thru 55 are the MSI image chips and the resulting minimum distance classified images of the remaining five areas within Iraq.

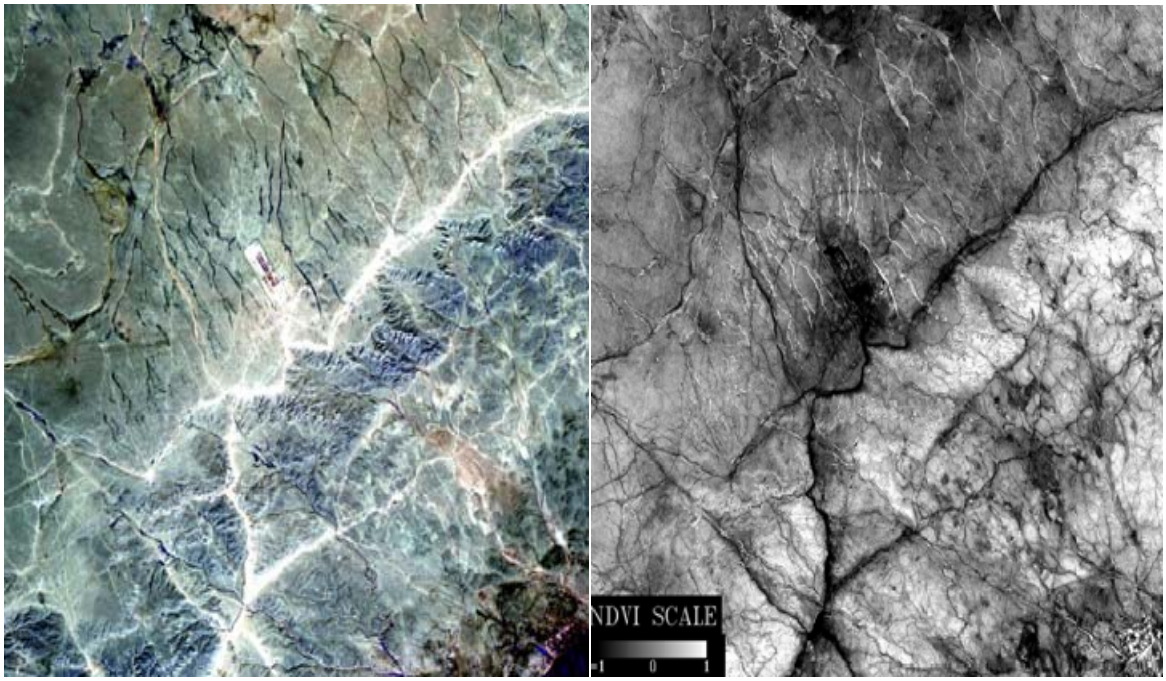

Figure 46. QuickBird MSI image of Abu-Dhakar taken 28 September 2006 and its NDVI transform.

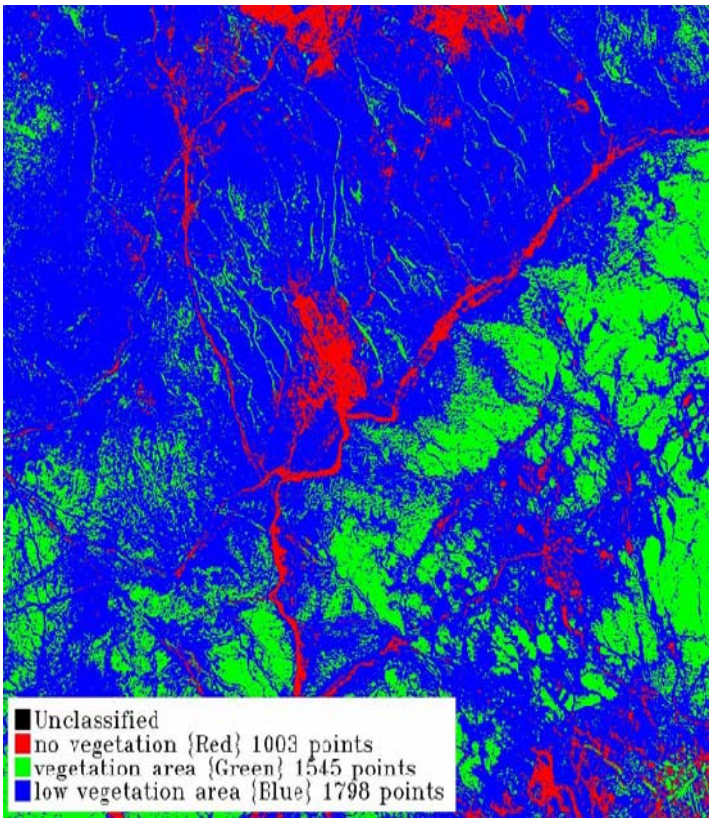

Figure 47. Minimum distance classified image of Abu-Dhakar.

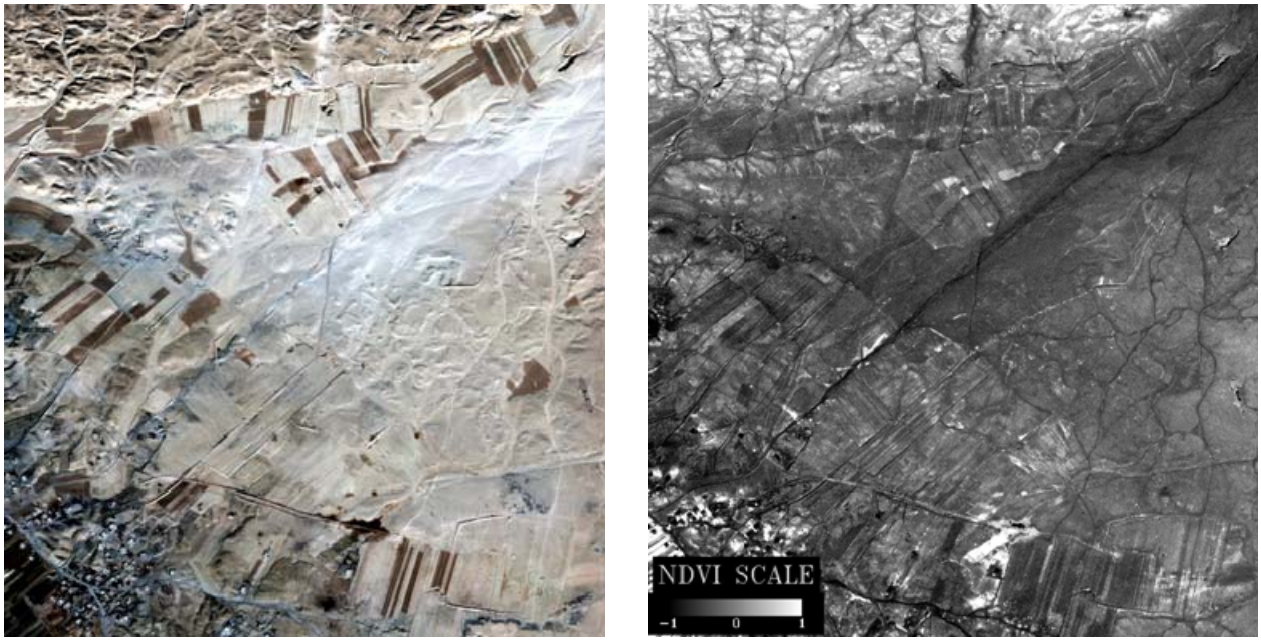

Figure 48. QuickBird MSI image of Al-Qaim taken 28 November 2004 and its NDVI transform.

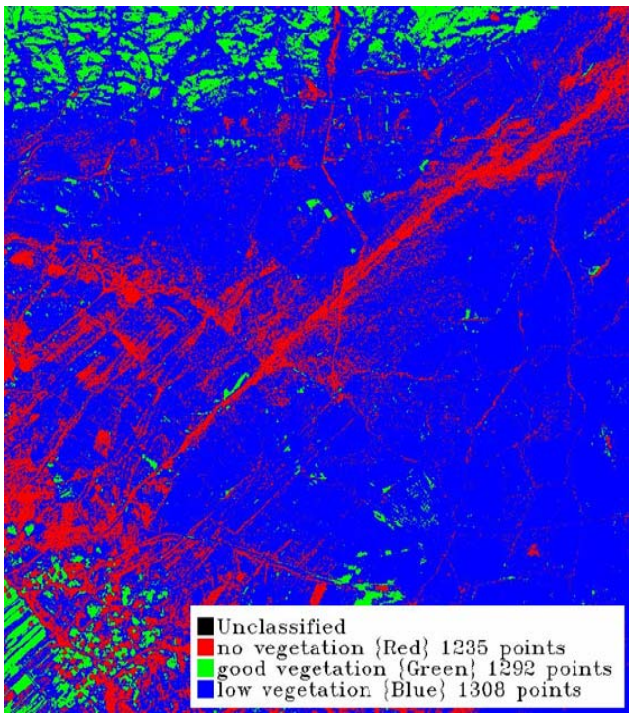

Figure 49. Minimum distance classified image of Al Qaim

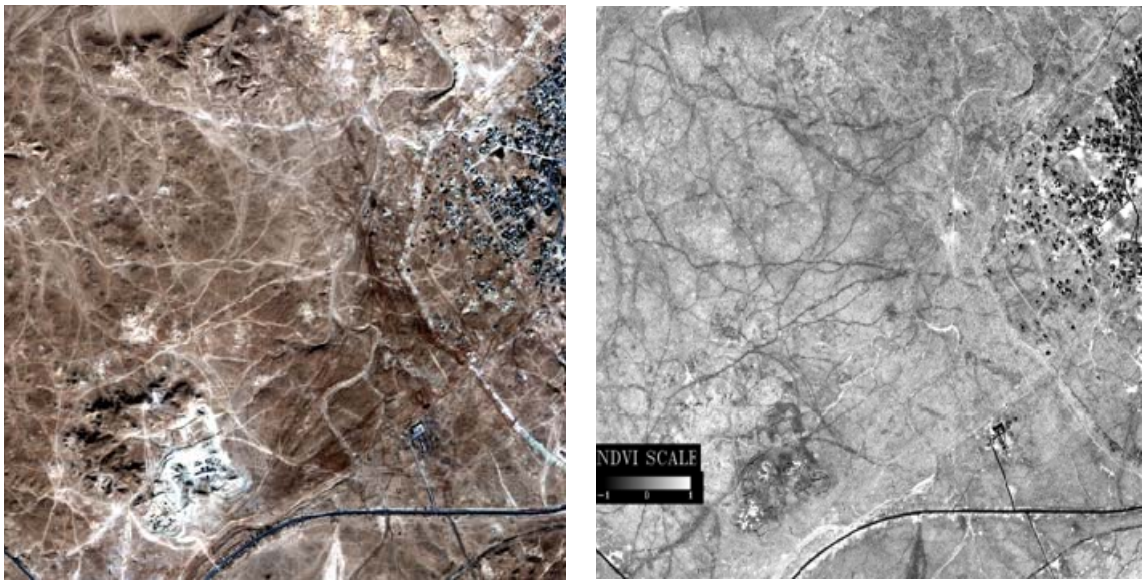

Figure 50. QuickBird MSI image of Anah taken 06 October 2006 and its NDVI transform

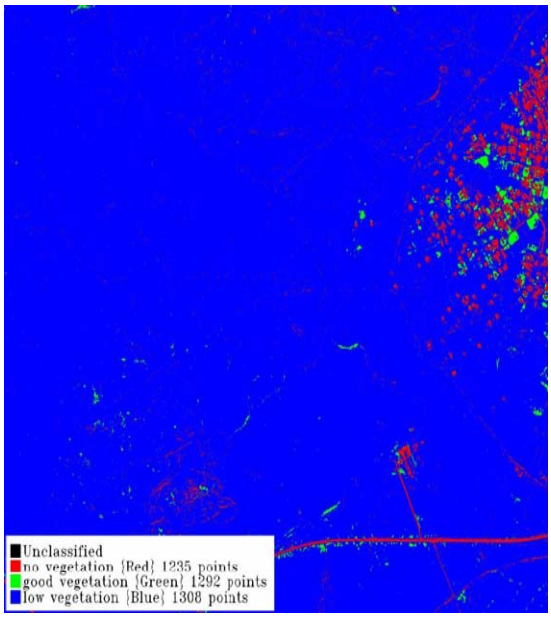

Figure 51. Minimum distance classified image of Anah.

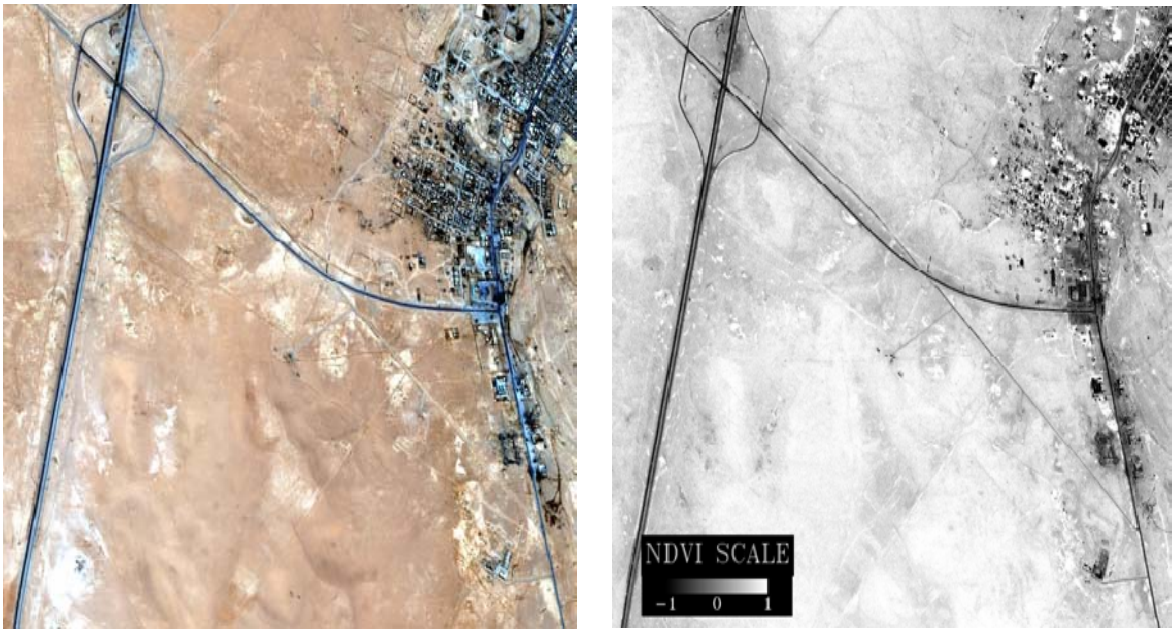

Figure 52. QuickBird MSI image of Ar-Rutbah taken 22 July 2004 and its NDVI transform.

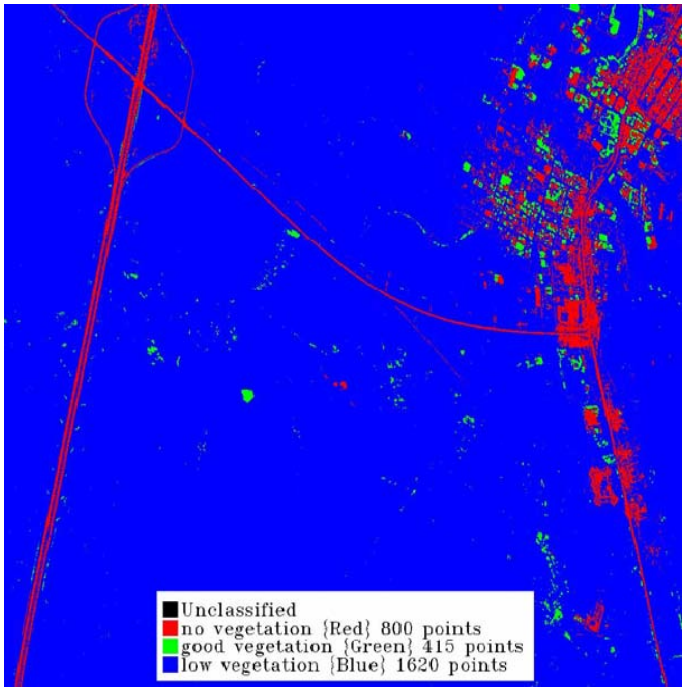

Figure 53. Minimum distance classified image of Ar-Rutbah.

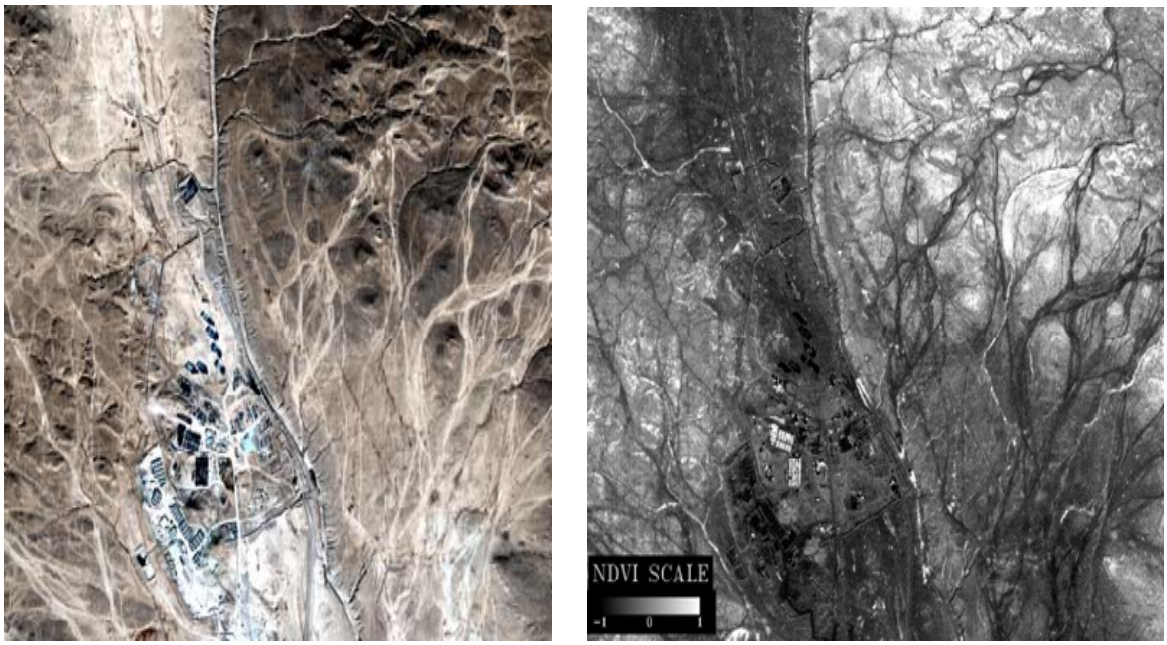

Figure 54. QuickBird MSI image of Rawah taken on 16 October 2006 and its NDVI transform

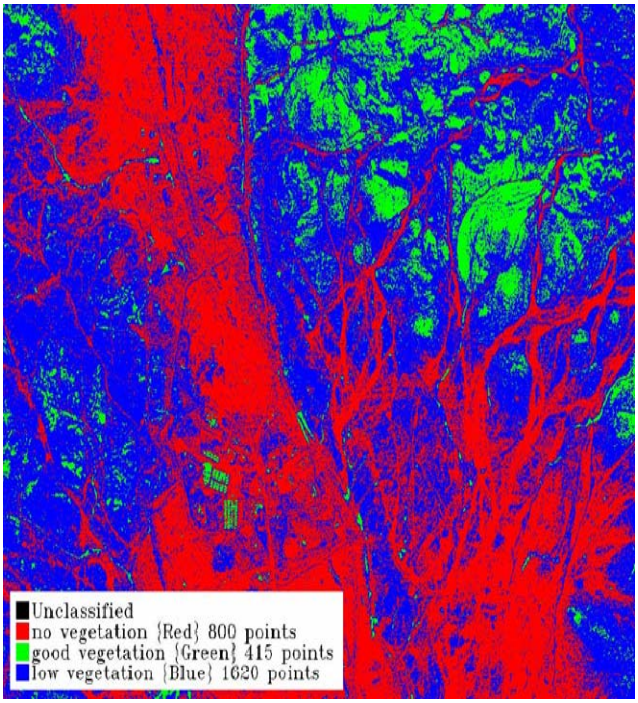

Figure 55. Minimum distance classified image of Rawah.

It was noticed that in the preceding figures that the bad landing zones were on what looks to be roads or highways in Iraq. The good landing zones were in patches where the healthiest vegetation resides. These good landing zones varied within each image some were concentrated in an area while others were spread out.

V. SUMMARY & CONCLUSIONS

A SUMMARY

Visible and infrared images were analyzed for the purpose of separating good and bad landing zones in desert environments. The main criteria is vegetation vs non-vegetated areas, with an intermediate class which is poorly defined at this point.

The technique studies were the use of data from the ASTER instrument on the Terra Satellite. VNIR data were used to calculate the vegetation index, NDVI. The thermal (LWIR) data were studied in both day and night observations for the same locations. The 15-m GSD resolution of the ASTER VNIR data made it just possible to determine locations in the multiple data sets, and to allow registration of the scenes analyzed. The 60-m resolution of the LWIR channels made those data relatively difficult to use for our purposes, but did allow for comparison of the VNIR and LWIR responses in the analysis area.

The analysis of the data emphasized the use of 2-D scatter plots that compared NDVI values and thermal band 14 of ASTER. Persistent features were found in such plots for the training area at YPG. Each scatter plot observed had an associated pixel cluster “bump” that corresponded to the plowed field/silt. It was also observed that the even though the scatter plots did not have the exact same shape the Regions of interest resided relatively in the same areas within the scatter plots. Using the regions of interest within the scatter plot the images were classified using both the NDVI and thermal bands. It showed that although the NDVI was the more useful band, the thermal bands still showed the ability to distinguish the plowed field from the background to some degree in all but one daytime thermal data set when using the maximum likelihood classifier.

QuickBird MSI data were also analyzed from a vegetation (NDVI) perspective. Following the pattern established using the ASTER data; NDVI images were classified by identifying darker areas as potential bad landing zones and lighter areas as potential good landing zones.

B CONCLUSION

In conclusion using the methodology described in this thesis civil remote sensing systems were successfully able to classify images of YPG. These classified images depicted where possible good and bad landing zone areas resided within the image. Cross checking the classified images with the actual ground truth showed that the ground truth bad landing zones and good landing zones coordinates held true within each classified image. This proved that civil systems in particular ASTER could be used to predict helicopter brownout areas at YPG.

The QuickBird MSI data that was analyzed for the 6 Iraqi sites illustrated the application of the NDVI calculation for a different sensor environment. This work appears to have shown that if only one band is available to do image classification on a given area it can still be done successfully. Using only the NDVI transform each Iraqi area of interest was successfully trained and classified such that one could predict where the possible good and bad landing zones were.

VI. RECOMMENDATIONS

A. VALIDATION

Further analysis into the use of ASTER's Visible Near IR and Thermal IR sensing instrument to discriminate brownout and non-brownout landing zones should be conducted to attempt to replicate the results that were found at Yuma Proving Ground. Analysis should be done on the MAWTS-1 site and the Indian Springs Sites.

As a test of the concepts applied and the conclusions drawn about the imagery analysis technique used to differentiate brownout from non brownout sites, consideration should be given to selecting sites not previously imaged or visited for evaluation. One option would be to choose sites near or on Edwards AFB, Camp Pendleton or FT Irwin. These bases are all located in California and two of them have Marine helicopter squadrons on station (Edwards and Camp Pendleton). The procedure would be to contact one of the squadrons and request a 5 kilometer square area that has known brownout and non brownout prone landing zones in it. It should be easily accessed easily by vehicle as well as helicopter in the event helicopter support is not available at the time of visit. The exact coordinates should not be known to the imagery evaluators, until after the site visit is completed which will confirm or deny the locations predicted through the BOA imagery analysis. Ideally a helicopter would be employed to test the various predicted landing zones with a follow-on interview of the aircrew for their assessment of the brownout conditions at those predicted landing zones.

B. BASELINE

Consideration should be given, for use in operational analysis to obtaining baseline MSI, IR and Radar data with respect to the dry season and the wet season of a potential operation area. This could allow comparison of data and imagery to possibly determine the degree to which the brownout conditions might be experienced. Using the

MSI and its associated NDVI versus Radar data would be idea to get a better understanding of how the different remote sensing instruments will detect possible brownout conditions.

ASTER data should be available for the analysis of Iraq landing zones. By having ASTER data available 2D scatter plots can be used using ASTER's TIR platform and QuickBird's MSI data. Ideally one would be present at the areas to be analyzed before the thin crust is broken, and photograph the first and consecutive landings to monitor the progression of the brownout condition with the deterioration of the landing zones. Finally for ease of use a program is being developed in Interactive Data Language (IDL) where the user just needs the NDVI image and a thermal image that will produce the same type of scatter plots that were used throughout this thesis. Using this program along with a digital elevation model will provide a good product for helicopter pilots landing in desert terrains.

LIST OF REFERENCES

Brady, Nyle C.and Weil, Ray R., Second Edition, Elements of Nature and Properties of Soils, Prentice Hall, 2004.

Brownout | California soil resource lab. Retrieved 8/10/2007, from http://casoilresource.lawr.ucdavis.edu/drupal/node/93.

Continuum Dynamics, Inc *CDI - products.* Retrieved 8/10/2007, from http://www.continuum-dynamics.com/pr-ldtran.html.

Digital Globe QuickBird Specifications. Retrieved 9/8/2007 from http://www.digitalglobe.com/about/quickbird.html.

Foth, Henry D. and Turk, Loyd M., Fifth Edition, Fundamentals of Soil Science, Wiley and Sons, Inc., 1972.

NASA Jet Propulsion Laboratory ASTER (2004). *Characteristics.* Retrieved 8/10/2007, from http://asterweb.jpl.nasa.gov/characteristics.asp.

——— ASTER *TIR.* Retrieved 8/10/2007, from http://asterweb.jpl.nasa.gov/tir.asp.

——— ASTER *Urban change.* Retrieved 8/10/2007, from http://asterweb.jpl.nasa.gov/content/03_data/05_Application_Examples/urban/.

——— ASTER VNIR. Retrieved 8/10/2007, from http://asterweb.jpl.nasa.gov/vnir.asp.

Olsen, R. C. (2007). *Remote sensing from air and space*. Bellingham, Wash.: SPIE Press.

Shewfelt, M. S. (2006). *Master's Thesis Naval Postgraduate School: Use of Remote Sensing in Predicting Helicopter Brownout Conditions*. September 2006 (Top Secret).

Tan, Kim H., First Edition, Enviromental Soil Science Marcel Dekker, Inc.

Wikipedia contributors. *Brownout (aviation).* Retrieved 8/10/2007, from http://en.wikipedia.org/wiki/brownout_(aviation)?oldid=147957179.

Yamaguchi, Y., Kahle, A. B., Tsu, H., Kawakami, T., & Pniel, M. (1998). Overview of advanced spaceborne thermal emission and reflection radiometer (ASTER). *Geoscience and Remote Sensing, IEEE Transactions on, 36*(4), 1062-1071.

THIS PAGE INTENTIONALLY LEFT BLANK

INITIAL DISTRIBUTION LIST

1. Defense Technical Information Center
   Ft. Belvoir, Virginia

2. Dudley Knox Library
   Naval Postgraduate School
   Monterey, California

3. Navy Research Lab (Code 7260)
   Washington D.C.

4. Navy TENCAP CNO N61R4
   2000 Navy
   Pentagon
   Washington D.C